

Gravitational Interaction of Ultralight Dark Matter with Interferometers

Hyungjin Kim*

Deutsches Elektronen-Synchrotron DESY, Notkestr. 85, 22607 Hamburg, Germany

Ultralight dark matter exhibits an order-one density fluctuation over the spatial scale of its wavelength. These fluctuations gravitationally interact with gravitational wave interferometers, leading to distinctive signals in detectors. We investigate the ultralight dark matter-induced effects in the gravitational wave interferometers. We perform a systematic computation of the power spectrum of ultralight dark matter in interferometers. We show that the ultralight dark matter-induced effect is most relevant for the interferometers with long baseline and that it is only a sub-leading effect compared to the estimated noise level in the case of Laser Interferometer Space Antenna or future interferometers with an arm-length comparable to a few astronomical units. Gravitational wave interferometers can then place upper limits on the ultralight dark matter density in the solar system. We find that, under certain assumptions, future interferometers with AU-scale arm-length might probe the dark matter density a few hundred times the local dark matter density, which is measured over a much larger spatial scale.

CONTENTS

I. Introduction	2
II. Ultralight dark matter	3
A. Density fluctuation	5
B. Metric fluctuation	6
III. Gravitational wave interferometers	7
A. Interferometry response	8
1. Michelson interferometer	8
2. Time-delay interferometer	9
B. ULDM signal	10
1. Deterministic signal	11
2. Stochastic signal	11
C. Application	12
1. LIGO	12
2. Einstein Telescope	13
3. LISA	13
4. μ Ares	14
5. Big Bang Observatory	14
IV. Discussion	14
V. Conclusion	15
Acknowledgments	16
A. Power spectrum	16
B. Induced phase	17
C. Density fluctuation	18
D. Coherent signals in pulsar timing array	19
References	20

* hyungjin.kim@desy.de

I. INTRODUCTION

Ultralight dark matter (ULDM) remains an attractive dark matter candidate. Its mass is smaller than several eV-scale, and it behaves like classical waves. The QCD axion is one of the most theoretically interesting ultralight dark matter candidates [1–6]. Other interesting candidates often arise from recent developments in dynamical solutions to the electroweak hierarchy problem [7–14]. Phenomenologically, ultralight dark matter of extremely small mass $m \sim 10^{-21}$ eV has also been actively investigated as it changes the prediction of cold dark matter at galactic and sub-galactic scales [15]. Being wave-like, such ultralight dark matter candidates lead to interesting phenomenology in the early and late universe. See Ref. [16] for a recent review on wave dark matter.

Recent numerical simulations of ultralight dark matter halo have observed an order one density fluctuation all over galaxies [17, 18]. The fluctuation is extended over the spatial scale given by the wavelength of dark matter. This characteristic density fluctuation can be intuitively understood in terms of *quasiparticles*, whose size (λ) and mass (m_{eff}) are given as its wavelength and the total mass enclosed within the volume of de Broglie wavelength [19]:

$$\lambda = \frac{1}{m\sigma} \simeq 10^2 \text{ pc} \left(\frac{10^{-22} \text{ eV}}{m} \right) \left(\frac{200 \text{ km/sec}}{\sigma} \right), \quad (1)$$

$$m_{\text{eff}} = \frac{\pi^{3/2} \rho_0}{(m\sigma)^3} \simeq 5 \times 10^4 M_\odot \left(\frac{\rho_0}{\text{GeV/cm}^3} \right) \left(\frac{10^{-22} \text{ eV}}{m} \right)^3 \left(\frac{200 \text{ km/sec}}{\sigma} \right)^3. \quad (2)$$

Here m is the mass of ULDM, ρ_0 is the mean dark matter density, and σ is the velocity dispersion. For $m \ll$ eV, the size and the mass of the quasiparticles could be astronomical.¹

These quasiparticles interact continuously with interferometers, designed to detect gravitational waves (GWs) of astrophysical and cosmological origin. Since they are engineered to measure an extremely small disturbance of spacetime due to GWs, any interaction of quasiparticles with such interferometers leaves some distinctive impacts on detectors. The main goal of this work is, therefore, to characterize the impacts of ULDM on gravitational wave interferometers. In particular, we ask two questions: (i) if ULDM signals can be larger than the projected noise level in each detector and (ii) if the dark matter density in the solar system can be probed only through the gravitational interaction of order-one density fluctuations of ULDM with detectors. We will address these questions by computing the signal power spectrum of ULDM in detectors and comparing it with the noise power spectrum of detectors.

Without detailed computation, we can already estimate the expected effects of ULDM and partially answer one of the above two questions. Consider an interferometer with two test masses. A useful quantity is a differential acceleration, $\Delta a = a_1 - a_2$, between two test masses induced by ULDM density fluctuations. Suppose that a quasiparticle is located right next to the first test mass. In this case, the differential acceleration is estimated as

$$\Delta a = a_1 - a_2 = \frac{Gm_{\text{eff}}}{\lambda^2} - \frac{Gm_{\text{eff}}}{(L + \lambda)^2} \simeq \bar{a} \min \left(1, \frac{2L}{\lambda} \right),$$

where L is a typical size of the interferometer and typical acceleration \bar{a} is defined as

$$\bar{a} \equiv \frac{Gm_{\text{eff}}}{\lambda^2} = \pi^{3/2} G \rho_0 \lambda. \quad (3)$$

As the mass m decreases (hence wavelength and effective mass increases), the differential acceleration increases until it saturates to $\bar{a} = 2G\rho_0 L$ when $\lambda = 2L$; when the size of a quasiparticle becomes comparable to the size of the interferometer. At this saturation point, we find $\Delta a \sim 10^{-28} \text{ m s}^{-2}$ for $L = 4 \text{ km}$ (LIGO/VIRGO), $\Delta a \sim 10^{-22} \text{ m s}^{-2}$ for $L = 2.5 \text{ M km}$ (LISA), and $\Delta a \sim 10^{-20}$ for $L = 400 \text{ M km}$ (e.g. μAres strawman mission concept [25] and Fedderke et al [26]). Here we use $\rho_0 = 0.4 \text{ GeV/cm}^3$.

This can be compared with the sensitivity of detectors. The strain noise power spectrum can be converted into the root-mean-square fluctuation of acceleration by $\Delta a \sim [S_n (2\pi f)^4 L^2 \Delta f]^{1/2}$. We find $\Delta a = 10^{-14} \text{ m s}^{-2}$ for LIGO with $f \sim \Delta f \sim 50 \text{ Hz}$, $\Delta a = 10^{-16} \text{ m s}^{-2}$ for LISA with $f \sim \Delta f \sim 0.1 \text{ mHz}$, and $\Delta a = 10^{-17} \text{ m s}^{-2}$ for μAres proposal with $f \sim \Delta f \sim$ a few $\times 10^{-7} \text{ Hz}$. For ground-based interferometers, the ULDM-induced noise is irrelevant as it is many orders of magnitude smaller than detector noises. For space-borne interferometers, the ULDM effect is a few orders of magnitude smaller than the mission-required detector noise level. We may conclude from this comparison that the ULDM effect in interferometers through gravitational interaction is unlikely to interfere with the operation

¹ The quasiparticle, however, is not a particle in a traditional sense. The density fluctuation is a result of wave interference, and it lasts only for a coherence time $\tau = 1/m\sigma^2$. In addition, the fluctuation of the mass within a fixed volume in galaxies follows the exponential distribution in the case of ULDM, while it is the Poisson distribution for the particle dark matter. These features make the behavior of ULDM qualitatively different from that of massive particle dark matter candidates, such as primordial black holes or massive compact halo objects, which have been previously studied in [20–24].

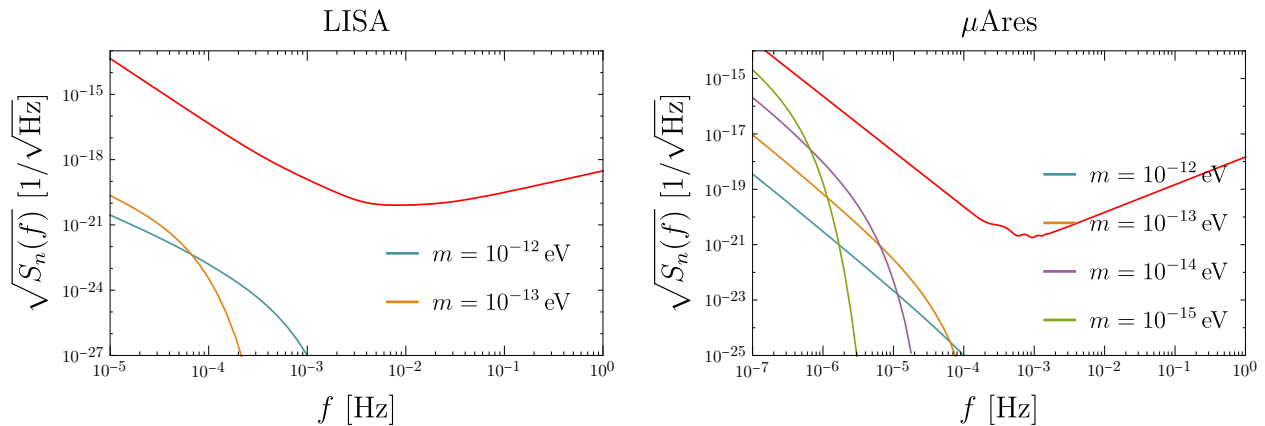


FIG. 1. The ultralight dark matter-induced noise for (left) LISA and (right) μ Ares proposal [25]. The red line is the required noise level for the mission. The other colored solid lines are the ultralight dark matter-induced noise for given masses. In both cases, the shown is the strain noise power spectrum in the Michelson-like TDI-X variable. Note that, for μ Ares, the low-frequency noise could be dominated by the gravity gradient noise as discussed in Ref. [27]. See the main text for details.

of interferometers for the detection of GWs. For a more correct comparison, however, we will need to compute the power spectrum of ultralight dark matter-induced effects since the above estimation on Δa does not carry any spectral information about the ULDM effects in the detector.

We summarize the main results here. From the detailed computation of the ULDM power spectrum, we find that the spectrum generally consists of two distinctive frequency components: one at $\omega = 2m$ and the other at $\omega < m\sigma^2$. This has interesting phenomenological implications as it offers different ways to search for ultralight dark matter signals. In Figure 1, we show the low-frequency part ($\omega < m\sigma^2$) of the ULDM signal. The ULDM noise is sub-dominant even for the interferometers with arm-lengths larger than a few million km, such as LISA and other proposals with arm-length comparable to astronomical units, confirming our order-of-magnitude estimation above. The interferometers then can be used to place an upper limit on the dark matter content in the solar system. Two distinct frequency components offer multiple ways for ULDM searches in interferometers. The $\omega = 2m$ component behaves similarly to a deterministic signal, which can be searched with the matched filter. The low-frequency ($\omega < m\sigma^2$) component, on the other hand, behaves similarly to the stochastic background, which can be searched by cross-correlating detector outputs if more than two detectors are available. The resulting constraints and projections on ρ/ρ_0 are shown in Figure 2, suggesting that the density of ULDM in the solar system, $\rho \sim \mathcal{O}(10^2)\rho_0$, could be probed with GW interferometers only through gravitational interaction.

The work is organized as follows. In section II, we review the basic statistical properties of ultralight dark matter and compute the spectrum of density contrast. This will establish a basis for the detailed investigation of the response of GW interferometers to the ULDM density fluctuations. In section III, we discuss how GW interferometers respond to the ULDM density fluctuation, and how the ultralight dark matter signal can be searched with the matched filter and with cross-correlation of detector outputs in cases where there are more than two detectors. In section IV, we discuss some of the assumptions that might affect our results. We conclude in section V. The natural unit ($c = \hbar = 1$) is used in this work.

II. ULTRALIGHT DARK MATTER

We review the basic statistical properties of ultralight dark matter in this section. We consider a scalar field minimally coupled to gravity without self-interaction. The ultralight dark matter field operator is given as

$$\hat{\phi}(x) = \sum_i \frac{1}{\sqrt{2mV}} (a_i e^{-ik_i \cdot x} + a_i^\dagger e^{ik_i \cdot x}),$$

where a_i and a_i^\dagger are annihilation and creation operator of the plane wave mode i , satisfying $[a_i, a_j^\dagger] = \delta_{ij}$. The continuum expression can be obtained by $\sum_i \rightarrow V \int d^3k / (2\pi)^3$, $a_i \rightarrow a(\vec{k})/\sqrt{V}$, $[a(\vec{k}), a^\dagger(\vec{q})] = (2\pi)^3 \delta^{(3)}(\vec{k} - \vec{q})$. For later convenience, we stick to the above discrete convention. Any deformation of wave function due to the gravitational potential of the Sun is ignored since this effect is at the level of $\mathcal{O}(1)\%$ for the halo dark matter [31].

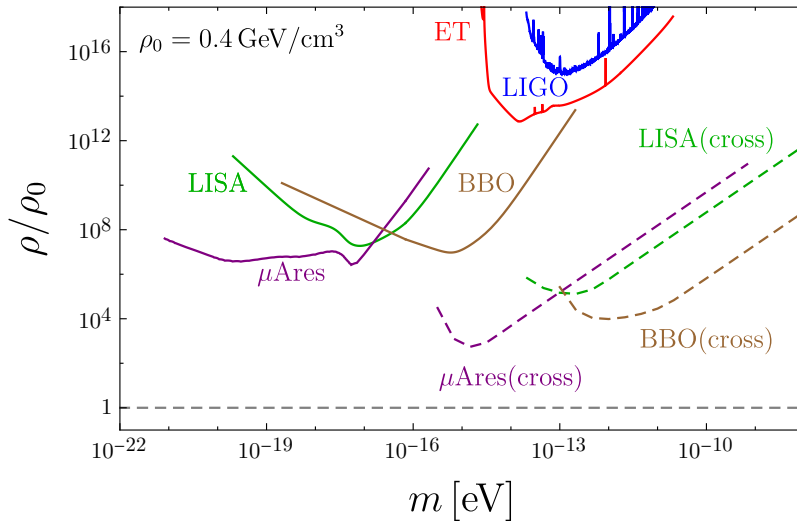


FIG. 2. The constraints and projections on dark matter density in the solar system. Here $\rho_0 = 0.4 \text{ GeV/cm}^3$ is the local dark matter density measured over $\gtrsim \mathcal{O}(100)$ pc scale (see e.g. [28, 29] for reviews). The solid lines are obtained from the matched filter for the coherently oscillating dark matter signal at $\omega = 2m$, while the dashed lines are obtained by cross-correlating signals in two detectors at $\omega < m\sigma^2$. Note that the current design of LISA does not include two detectors, but other spaceborne interferometer proposals, such as TianQin or Taiji, would potentially allow the cross-correlation searches [30]. For the matched filter search of the coherently oscillating signal, we take for simplicity vanishing dark matter velocity $v_0 = 0$; we check this approximation does not change the numerical result in a significant way. For the stochastic signal search with the cross-correlation, we take an average of the signal over twelve months. See the main text for details.

The statistical property of ultralight dark matter is defined by the density operator. The density operator is $\hat{\rho} = \prod_i \hat{\rho}_i \otimes$ where $\hat{\rho}_i$ is the density operator of each mode, given by [31]

$$\hat{\rho}_i = \int d^2\alpha_i p(\alpha_i) |\alpha_i\rangle \langle \alpha_i|. \quad (4)$$

Here $|\alpha_i\rangle$ is the coherent state, satisfying $a_i|\alpha_i\rangle = \alpha_i|\alpha_i\rangle$ ($\alpha_i \in \mathbb{C}$), and the quasi-probability distribution $p(\alpha_i)$ is given as

$$p(\alpha_i) = \frac{1}{\pi f_i} \exp\left[-\frac{|\alpha_i|^2}{f_i}\right]. \quad (5)$$

The f_i is the mean occupation number for the mode i . This quasi-probability distribution function $p(\alpha_i)$ corresponds to the Rayleigh distribution for the amplitude, $|\alpha_i|$, and the uniform distribution for the phase, $\arg(\alpha_i)$ [32–34]. With this description, any n -point correlation function of an operator $\hat{\mathcal{O}}$ can be easily computed by the trace operation, $\langle \mathcal{O} \rangle = \text{Tr}(\mathcal{O}\hat{\rho})$. In the large occupation number limit, the operators (a_i, a_i^\dagger) can be replaced by commuting complex random number (α_i, α_i^*) , whose probability distribution is given by (5).

It is useful to note the ensemble averages of the creation and annihilation operators:

$$\langle a_i a_j^\dagger \rangle = \langle a_i^\dagger a_j \rangle = f_i \delta_{ij}, \quad \text{and} \quad \langle a_i a_j a_k^\dagger a_\ell^\dagger \rangle = f_i f_j (\delta_{ik} \delta_{j\ell} + \delta_{i\ell} \delta_{jk}). \quad (6)$$

Here we approximate a_i and a_i^\dagger as a commuting random complex number α_i and α_i^* , whose underlying distribution follows the quasi-probability distribution $p(\alpha_i)$. The ultralight dark matter field defined with (5) is a Gaussian random field, and therefore, the ensemble average of any operators with $N(a) - N(a^\dagger) \neq 0$ vanishes, where $N(a)$ and $N(a^\dagger)$ are the number of annihilation and creation operator, respectively.

The energy density of the ultralight dark matter is

$$\begin{aligned} \rho_\phi &= \frac{1}{2} \left[\dot{\phi}^2 + (\nabla\phi)^2 + m^2\phi^2 \right] \\ &= \frac{1}{2V} \sum_{i,j} \frac{1}{\sqrt{2\omega_i}\sqrt{2\omega_j}} \left[W_{ij}^- \left(a_i a_j e^{-i(k_i+k_j)\cdot x} + a_i^\dagger a_j^\dagger e^{i(k_i+k_j)\cdot x} \right) + W_{ij}^+ \left(a_i a_j^\dagger e^{-i(k_i-k_j)\cdot x} + a_i^\dagger a_j e^{i(k_i-k_j)\cdot x} \right) \right]. \quad (7) \end{aligned}$$

For notational simplicity, we have introduced W_{ij}^\pm , defined as

$$W_{ij}^\pm = m^2 \pm (\omega_{k_i} \omega_{k_j} + \vec{k}_i \cdot \vec{k}_j) \approx 2m^2 \times \begin{cases} 1 & \text{for } W_{ij}^+ \\ -\frac{1}{4}(\vec{v}_i + \vec{v}_j)^2 & \text{for } W_{ij}^- \end{cases} \quad (8)$$

where the second expression holds in the non-relativistic limit. The mean energy density in the non-relativistic limit is

$$\langle \rho_\phi \rangle \equiv \rho_0 \approx \frac{m}{V} \sum_i f_i = m \int \frac{d^3k}{(2\pi)^3} f(\vec{k}) = m \int d^3v f(\vec{v}), \quad (9)$$

By taking the continuum limit, we reproduce the usual expression for the local dark matter density. In the last line, we change the integration variable to the velocity. The above expression fixes the normalization of the mean occupation number $f(\vec{v})$ used in this work.

A. Density fluctuation

Let us consider the density fluctuation, $\delta\rho_\phi = \rho_\phi - \rho_0$. The mean value vanishes $\langle \delta\rho_\phi \rangle = 0$. The correlator is

$$\langle \delta\rho_\phi(x) \delta\rho_\phi(y) \rangle = \int \frac{d^4k}{(2\pi)^4} e^{-ik \cdot (x-y)} P_{\delta\rho}(k),$$

where the power spectrum is defined as $\langle \delta\rho_\phi(k) \delta\rho_\phi^*(k') \rangle = (2\pi)^4 \delta^{(4)}(k - k') P_{\delta\rho}(k)$ and given by

$$P_{\delta\rho}(\omega, \vec{k}) = \frac{(2\pi)^4}{2} \int d\Pi_1 d\Pi_2 f(\vec{p}_1) f(\vec{p}_2) \times \left[(W_{12}^-)^2 (\delta^{(4)}(k - p_1 - p_2) + \delta^{(4)}(k + p_1 + p_2)) + (W_{12}^+)^2 (\delta^{(4)}(k - p_1 + p_2) + \delta^{(4)}(k + p_1 - p_2)) \right]. \quad (10)$$

This can be straightforwardly computed by using (5) and (7). Here $d\Pi = [d^3p/(2\pi)^3](2E)^{-1}$ is the Lorentz invariant phase space measure. In the frequency space, the correlator is

$$\langle \tilde{\delta\rho}_\phi(\omega, \vec{x}) \tilde{\delta\rho}_\phi^*(\omega', \vec{y}) \rangle = (2\pi) \delta(\omega - \omega') S_{\delta\rho}(\omega, \vec{L}), \quad (11)$$

where $\vec{L} = \vec{x} - \vec{y}$ and the power spectrum $S_{\delta\rho}(\omega, \vec{L})$ is given by

$$S_{\delta\rho}(\omega, \vec{L}) = \int \frac{d^3k}{(2\pi)^3} e^{i\vec{k} \cdot \vec{L}} P_{\delta\rho}(\omega, \vec{k}). \quad (12)$$

This power spectrum $S_{\delta\rho}(\omega, \vec{L})$ in the frequency space turns out to be more useful for the study of the response of GW interferometers to the ULDM fluctuations.

To illustrate the statistical properties of density contrast, we explicitly compute $S_\delta(\omega, \vec{0})$. We consider the normal distribution for dark matter velocity distribution,

$$f(\vec{v}) = \frac{\rho_0/m}{(2\pi\sigma^2)^{3/2}} \exp\left[-\frac{(\vec{v} - \vec{v}_0)^2}{2\sigma^2}\right], \quad (13)$$

where \vec{v}_0 is the mean dark matter velocity, and σ is the velocity dispersion. We work in the rest frame of the GW detectors. In general, $\vec{v}_0 \neq 0$ in this frame, but for the sake of simplicity, we take the isotropic limit $\vec{v}_0 = 0$ for now. Normalization of $f(\vec{v})$ is fixed by (9). Using (10) and (12), we find

$$S_\delta(\omega, \vec{0}) = \tau \left[\sigma^4 A_\delta(\omega) + B_\delta(\omega) \right], \quad (14)$$

where $\delta = \delta\rho_\phi/\rho_0$ is density contrast, and $\tau = 1/m\sigma^2 = 1/\omega_0$ is the coherence time. In the isotropic limit ($v_0/\sigma \ll 1$), the $A_\delta(\omega)$ and $B_\delta(\omega)$ are given by

$$A_\delta(\omega) = \frac{5\pi}{32} \left(\frac{\bar{v}}{\sigma}\right)^8 \exp\left[-\frac{\bar{v}^2}{\sigma^2}\right] \theta(\bar{v}^2) + (\omega \rightarrow -\omega), \quad (15)$$

$$B_\delta(\omega) = 2|\bar{\omega}| K_1(|\bar{\omega}|), \quad (16)$$

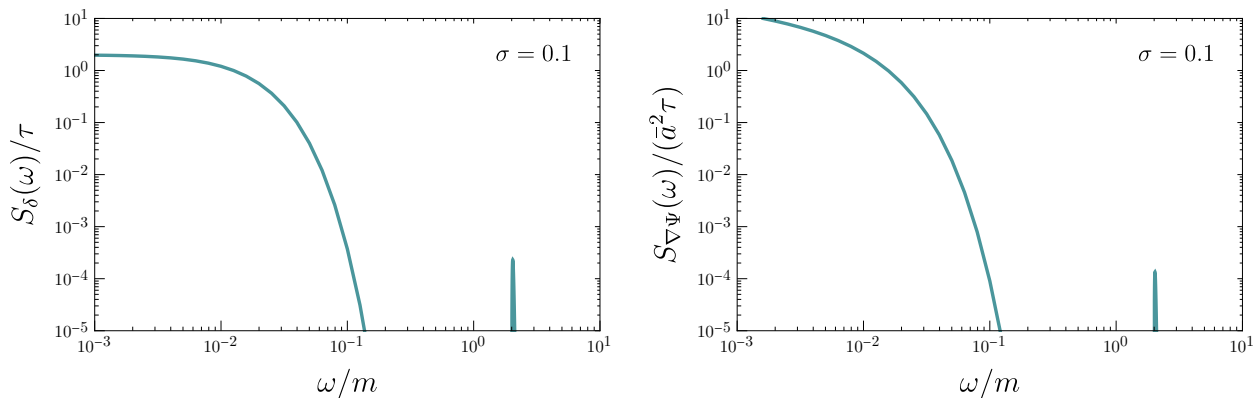


FIG. 3. (Left) the density contrast spectrum $S_\delta(\omega) = S_\delta(\omega, \vec{0})$ in the isotropic limit $v_0 = 0$. (Right) the spectrum for the gradient of the metric fluctuation, $S_{\nabla\Psi}(\omega) = \delta^{ij} S_{\nabla\Psi}^{ij}(\omega, \vec{0})$. Both spectra exhibit two distinctive frequency components: one at $\omega = 2m$ and another at $\omega < m\sigma^2$. For demonstration, we choose unrealistically large velocity dispersion $\sigma = 0.1$. The narrow peak at $\omega = 2m$ is suppressed by σ^4 compared to the smooth low-frequency spectrum. For $S_{\nabla\Psi}$, there is a logarithmic divergence at low frequencies due to the long-range nature of gravitational force.

where $K_n(x)$ is the modified Bessel function. Here we introduce, for notational simplicity,

$$\bar{v}^2(\omega) = (\omega/m - 2), \quad \text{and} \quad \bar{\omega} = \omega/(m\sigma^2) = \omega/\omega_0. \quad (17)$$

The spectrum $S_\delta(\omega, \vec{0})$ for $\vec{v}_0 = 0$ and $\sigma = 0.1$ is shown in the left panel of Figure 3.

This computation reveals an interesting feature in the ULDM density fluctuation. The spectrum contains two distinctive frequency components: a narrow peak at $\omega = 2m$ represented by $A_\delta(\omega)$ and a broad low-frequency spectrum at $\omega < m\sigma^2$ represented by $B_\delta(\omega)$. Both of them have a width $\Delta\omega \sim m\sigma^2$. They can be understood by investigating the energy density of a single mode, $\phi(t, \vec{x}) = \phi_0 \cos(\omega t - \vec{k} \cdot \vec{x})$,

$$\rho_\phi = \frac{1}{2} \left[\dot{\phi}^2 + (\nabla\phi)^2 + m^2\phi^2 \right] \approx \rho_0 \left[1 - v^2 \cos(2mt + \varphi) \right].$$

It consists of dc mode, which is what constitutes the low-frequency part ($\omega < m\sigma^2$) for a realistic multi-mode density contrast, and a coherently oscillating part which constitutes a spectrum at $\omega = 2m$ with its amplitude suppressed by v^2 . This v^2 suppression is responsible for a relative suppression of σ^4 in front of $A_\delta(\omega)$ in (14). These two distinctive frequency components in the density contrast remain in the ULDM-induced signal/noise power spectrum for the gravitational detectors, offering multiple ways to search for ultralight dark matter at a different mass range.

B. Metric fluctuation

ULDM fluctuations source metric perturbations. The metric is given by

$$ds^2 = (1 + 2\Phi)dt^2 - (1 - 2\Psi)dx^2. \quad (18)$$

These metric fluctuations perturb the position of test masses in interferometers and induce a time delay of light. Suppose a test mass at the position \vec{x} . The test mass acceleration and the metric fluctuations satisfy

$$\vec{a} = -\nabla\Phi, \quad (19)$$

$$\nabla^2\Psi = 4\pi G\delta\rho_\phi, \quad (20)$$

$$6\ddot{\Psi} + 2\nabla^2(\Phi - \Psi) = 24\pi G\delta P_\phi. \quad (21)$$

Here δP_ϕ is the pressure perturbation of the scalar field ϕ . The pressure of the field is $P_\phi = \dot{\phi}^2/2 - (\nabla\phi)^2/6 - m^2\phi^2/2$. Statistical properties of metric fluctuation as well as test mass position can be derived from those of ULDM by solving the above equations.

The relation between test mass acceleration, metric perturbations, and ULDM fluctuations becomes transparent in Fourier space:

$$\tilde{a}^i(k) = -ik^i \tilde{\Phi}(k), \quad (22)$$

$$\tilde{\Psi}(k) = -\frac{4\pi G}{k^2} \tilde{\delta\rho}_\phi(k), \quad (23)$$

$$\tilde{\Phi}(k) = -\frac{4\pi G}{k^2} \left[\left(1 - \frac{3\omega^2}{k^2}\right) \tilde{\delta\rho}_\phi(k) + 3\tilde{\delta P}_\phi(k) \right]. \quad (24)$$

From above, one can derive the relation between power spectra, e.g. $P_\Psi(k) = (4\pi G/k^2)^2 P_{\delta\rho}(k)$ and $P_a^{ij}(k) = k^i k^j P_\Phi(k)$, where the test mass acceleration power spectrum is defined as $\langle \tilde{a}^i(k) \tilde{a}^{j*}(k') \rangle = (2\pi)^4 \delta^{(4)}(k - k') P_a^{ij}(k)$.

Among others, the power spectrum of $\nabla\Psi$ turns out to be particularly useful for the later discussion. In the frequency space, it is given by

$$S_{\nabla\Psi}^{ij}(\omega, \vec{L}) = \int \frac{d^3k}{(2\pi)^3} e^{i\vec{k}\cdot\vec{L}} k^i k^j P_\Psi(k) = \bar{a}^2 \tau [\sigma^4 A^{ij} + B^{ij}] \quad (25)$$

where A^{ij} and B^{ij} are

$$A^{ij}(\omega, \vec{L}) = 16 \left(\frac{\bar{v}}{\sigma}\right)^6 \exp\left[-\frac{v_0^2 + \bar{v}^2}{\sigma^2}\right] \theta(\bar{v}^2) \left[\delta^{ij} \frac{I_3(X)}{X^3} + X^i X^j \frac{I_4(X)}{X^4} \right] + (\omega \rightarrow -\omega), \quad (26)$$

$$B^{ij}(\omega, \vec{L}) = \frac{2}{\sqrt{\pi}} \int_{-\infty}^{\infty} ds \frac{e^{-is\bar{\omega}}}{\sqrt{1+s^2}} \left[\delta^{ij} \frac{\text{erf}(Y) - G(Y)}{Y} + \frac{Y^i Y^j}{Y^3} (3G(Y) - \text{erf}(Y)) \right], \quad (27)$$

with $G(X) = [1/(2X^2)](\text{erf}(X) - 2Xe^{-X^2}/\sqrt{\pi})$ and

$$\vec{X} = 2\frac{\bar{v}}{\sigma} \left(\frac{\vec{v}_0}{\sigma} + i\vec{L}_\lambda\right), \quad \vec{Y} = \frac{1}{\sqrt{1+s^2}} \left(\frac{s\vec{v}_0}{\sigma} + \vec{L}_\lambda\right), \quad \vec{L}_\lambda = m\sigma\vec{L}. \quad (28)$$

The \bar{v} and $\bar{\omega}$ are defined in (17). Here I_n is the modified Bessel function of the first kind. Recall that $\tau = 1/m\sigma^2$, $m_{\text{eff}} = \pi^{3/2} \rho_0 / (m\sigma)^3$, and $\lambda = (m\sigma)^{-1}$ and the typical acceleration $\bar{a} = Gm_{\text{eff}}/\lambda^2$. We will see shortly that the response of the GW interferometer depends mostly on $\nabla\Psi$, and the above power spectrum can be used as a basic building block to study the response of interferometers to the ultralight dark matter fluctuations.

The structure of the spectrum is similar to the density contrast spectrum (14) since Ψ inherits its properties from ULDM fluctuations. Especially, $A^{ij}(\omega, \vec{L})$ is centered at $\omega = 2m$, while $B^{ij}(\omega, \vec{L})$ is spread over $\omega \lesssim m\sigma^2$. In the isotropic ($v_0 = 0$) and the long-wavelength limit ($m\sigma L \ll 1$), the A^{ij} and B^{ij} are simplified to

$$A_0^{ij}(\omega) \approx \frac{1}{3} \left(\frac{\bar{v}}{\sigma}\right)^6 \exp\left[-\frac{\bar{v}^2}{\sigma^2}\right] \theta(\bar{v}^2) \left[\delta^{ij} - \frac{(m\bar{v}L)^2}{4} (\delta^{ij} + 2\hat{L}^i \hat{L}^j) \right] + (\omega \rightarrow -\omega), \quad (29)$$

$$B_0^{ij}(\omega) \approx \frac{16}{3\pi} \left[\delta^{ij} K_0(|\bar{\omega}|) - \frac{(m\sigma L)^2}{5} (\delta^{ij} + 2\hat{L}^i \hat{L}^j) |\bar{\omega}| K_1(|\bar{\omega}|) \right]. \quad (30)$$

The spectrum $S_{\nabla\Psi}(\omega) = \delta^{ij} S_{\nabla\Psi}^{ij}(\omega, \vec{0})$ is shown in the right panel of Figure 3. Naively, this can be considered as a test mass acceleration power spectrum. While the overall structure of the spectrum is similar, the acceleration spectrum logarithmically diverges at small ω . More specifically, $B_0^{ij} \propto \delta^{ij} \ln(1/|\bar{\omega}|)$ for $\bar{\omega} \ll 1$, and this logarithmic divergence is related to the long-range nature of the gravitational interaction. The derivation of $B^{ij}(\omega, \vec{L})$ is given in Appendix A.

III. GRAVITATIONAL WAVE INTERFEROMETERS

To investigate how each interferometer responds to the ULDM fluctuation, we first consider a simple setup shown in Figure 4 where a phase-coherent laser begins from TM0, reaches TM1, and returns to TM0 again at t . The phase of the laser at time t is given by

$$e^{-i\omega_L t_0} = e^{-i\omega_L t} e^{2ik_L L} e^{i\Delta\phi},$$

since the phase along the null trajectory does not change. Here (ω_L, \vec{k}_L) is the laser frequency and wave vector, and t_0 is the time at which the laser begins from TM0. Since $t_0 = t - 2L$, the laser acquires additional phase $e^{2ik_L L}$ during this one round-trip.

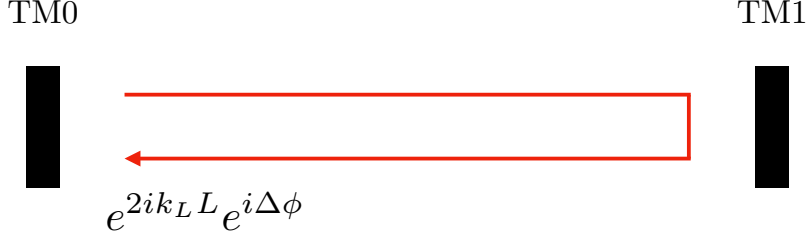


FIG. 4. The laser begins at t_0 at TM0. It propagates to TM1 and returns to TM0 at time t . During one round-trip, the laser acquires a phase $e^{2ik_L L}$ without ultralight dark matter. With ultralight dark matter, additional phase $e^{i\Delta\phi} = e^{2i\omega_L(\delta t + \delta L)}$ is induced because of (i) time-delay δt of the laser light and (ii) the fluctuation of the distance between two test masses δL .

Ultralight dark matter introduces an additional phase in two different ways: it introduces the time delay of laser light and it perturbs the test mass position. The additional phase $e^{i\Delta\phi}$ is introduced as a result, and it is given by

$$\Delta\phi(t) = 2\omega_L(\delta t + \delta L) \quad (31)$$

where the test mass perturbation δL and the time delay δt are given as

$$\delta L = +\frac{1}{2}\hat{x} \cdot \left[(\delta\vec{x}_1(t-L) - \delta\vec{x}_0(t-2L)) + (\delta\vec{x}_1(t-L) - \delta\vec{x}_0(t)) \right], \quad (32)$$

$$\delta t = -\frac{1}{2} \left[\int_{t-L}^t dt' + \int_{t-2L}^{t-L} dt' \right] [\Psi(t', \vec{x}(t')) + \Phi(t', \vec{x}(t))], \quad (33)$$

where $\delta\vec{x}_0$ and $\delta\vec{x}_1$ are the perturbation of the position of TM0 and TM1 around their nominal positions, \vec{x}_0 and \vec{x}_1 . Note that the argument $\vec{x}(t')$ in the metric perturbation must be computed along the null trajectory. The above expression is obtained by solving null geodesic with the metric perturbation; specifically, one finds $t_0 = t - 2(L + \delta L) - 2\delta t$.

The additional phase $\Delta\phi$ can be expanded in terms of metric perturbations in the Fourier space. In particular, it can be approximated as

$$\widetilde{\Delta\phi}(\omega) \approx \pm \frac{\omega_L}{\omega^2} e^{i\omega L} \int \frac{d^3k}{(2\pi)^3} e^{i\vec{k} \cdot \vec{x}_0} [i\vec{k} \cdot \vec{D}(\hat{n}, L)] \widetilde{\Psi}(k), \quad (34)$$

where $\hat{n} = (\vec{x}_1 - \vec{x}_0)/L$ and the vector $\vec{D}(\hat{n}, L) = 2\hat{n}[e^{i\vec{k} \cdot \hat{n}L} - \cos(\omega L)]$ encodes the response of this simple system to the ULDM fluctuations. The detailed derivation of the expression is given in Appendix B.

A. Interferometry response

1. Michelson interferometer

Consider now the Michelson interferometer. The Michelson interferometer consists of two arms. The laser combines at the asymmetric output, and the resulting power is $P = P_0 \sin^2(k_L \Delta L + \Delta\phi_{\text{Mich}})$ where $\Delta\phi_{\text{Mich}} = \frac{1}{2}(\Delta\phi_x - \Delta\phi_y)$ with the additional phase $\Delta\phi_{x,y}$ acquired by the laser that has propagated along x - and y -arm, respectively. The expression for $\Delta\phi_{x,y}$ is given in (34). In the frequency space, the phase is

$$\widetilde{\Delta\phi}_{\text{Mich}}(\omega) = \pm \frac{\omega_L}{\omega^2} e^{i\omega L} \int \frac{d^3k}{(2\pi)^3} e^{i\vec{k} \cdot \vec{x}_0} [i\vec{k} \cdot \vec{D}_{\text{Mich}}(\hat{x}, \hat{y}, L)] \widetilde{\Psi}(k) \quad (35)$$

where $\vec{D}_{\text{Mich}}(\hat{x}, \hat{y}; L) = \frac{1}{2}[\vec{D}(\hat{x}, L) - \vec{D}(\hat{y}, L)]$ is the response vector of the Michelson interferometer, and \vec{x}_0 is the beam splitter position. For simplicity, we assume an equal arm-length.

The power spectrum for differential arm-length $\widetilde{\Delta L}/L = \widetilde{\Delta\phi}_{\text{Mich}}/(\omega_L L)$ can be directly obtained from the above expression, and it is given by

$$S_{\Delta L/L}^{\text{ULDM}}(\omega) = \frac{1}{\omega^4 L^2} \int \frac{d^3k}{(2\pi)^3} |\vec{k} \cdot \vec{D}_{\text{Mich}}|^2 P_{\Psi}(k) = \frac{\bar{a}^2}{\omega^4 L^2} \tau [\sigma^4 A_{\text{Mich}} + B_{\text{Mich}}]. \quad (36)$$

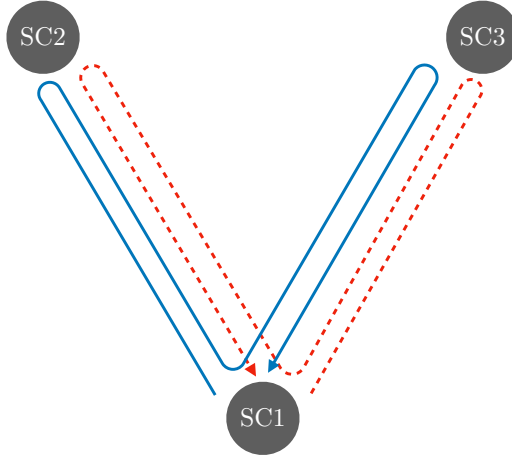


FIG. 5. A cartoon for the time-delay interferometer. Each spacecraft is loaded with two proof masses. The Michelson-like X variable measures the phase difference of the laser along two paths shown as blue and red dashed lines.

The detector response is encoded in the function A_{Mich} and B_{Mich} . Note again the similar structure of the power spectrum compared to the density contrast and metric fluctuation $\nabla\Psi$. The A_{Mich} and B_{Mich} can be decomposed in terms of A^{ij} and B^{ij} in (25) as follows:

$$A_{\text{Mich}}(\omega; \hat{x}, \hat{y}, L) = 2 \left[\frac{1 + \cos^2(\omega L)}{2} (A_R^{11}(\vec{0}) + A_R^{22}(\vec{0})) - \cos(\omega L) (A_R^{11}(\vec{x}_1) + A_R^{22}(\vec{x}_2)) \right. \\ \left. - (A_R^{12}(\vec{x}_{12}) + \cos^2(\omega L) A_R^{12}(\vec{0}) - \cos(\omega L) (A_R^{12}(\vec{x}_1) + A_R^{12}(\vec{x}_2))) \right], \quad (37)$$

$$B_{\text{Mich}}(\omega; \hat{x}, \hat{y}, L) = 2 \left[\frac{1 + \cos^2(\omega L)}{2} (B_R^{11}(\vec{0}) + B_R^{22}(\vec{0})) - \cos(\omega L) (B_R^{11}(\vec{x}_1) + B_R^{22}(\vec{x}_2)) \right. \\ \left. - (B_R^{12}(\vec{x}_{12}) + \cos^2(\omega L) B_R^{12}(\vec{0}) - \cos(\omega L) (B_R^{12}(\vec{x}_1) + B_R^{12}(\vec{x}_2))) \right], \quad (38)$$

where $A_R^{ab} = \hat{x}_a^i \hat{x}_b^j A_R^{ij}$, $B_R^{ab} = \hat{x}_a^i \hat{x}_b^j B_R^{ij}$,

$$A_R^{ij}(\vec{x}) = \frac{1}{2} [A^{ij}(\vec{x}) + A^{ij}(-\vec{x})], \quad \text{and} \quad B_R^{ij}(\vec{x}) = \frac{1}{2} [B^{ij}(\vec{x}) + B^{ij}(-\vec{x})].$$

Here $(\hat{x}_1, \hat{x}_2) = (\hat{x}, \hat{y})$ denote the unit vector to each arm. The dependence of A_R^{ab} on ω is suppressed in the above expression for notational simplicity. This power spectrum can be compared with the noise power spectrum in the current and future ground-based interferometers, such as LIGO and Einstein Telescope. While we only discuss the Michelson interferometer here, the response of Fabry-Pérot Michelson interferometer is the same up to the overall multiplication factor.

The response functions can be simplified in the isotropic ($v_0/\sigma \ll 1$) and long-wavelength limit ($m\sigma L \ll 1$). In such limits, they become

$$A_{\text{Mich}} \approx \frac{8}{3} \left(\frac{\bar{v}}{\sigma} \right)^6 \theta(\bar{v}^2) e^{-(\bar{v}/\sigma)^2} \left[\sin^4 \left(\frac{\omega L}{2} \right) + \frac{(m\bar{v}L)^2}{4} \left(\cos \omega L - \sin^2 \left(\frac{\omega L}{2} \right) \right) \right] + (\omega \rightarrow -\omega), \quad (39)$$

$$B_{\text{Mich}} \approx \frac{128}{15\pi} |\bar{\omega}| K_1(|\bar{\omega}|) (m\sigma L)^2. \quad (40)$$

In this limit, one sees $B_{\text{Mich}} \propto (m\sigma L)^2 = (L/\lambda)^2$, which signals the tidal limit of differential acceleration as estimated in the introduction. On the other hand, for A_{Mich} , the prefactor strongly supports $\omega = 2m$. The first term $\sin^4(\omega L/2)$ dominates the second term as long as $m\sigma L \gtrsim \sigma^2$.

2. Time-delay interferometer

Let us now consider the time-delay interferometer. We take LISA as a benchmark for the discussion. The constellation consists of three spacecraft (SC₁, SC₂, SC₃) with three arms, and in each arm, two Doppler shift measurements

are carried out; in this simplified picture, there are six one-way Doppler shift measurements. For a detailed discussion of the time-delay interferometer, we refer readers to Refs. [35, 36].

A single one-way Doppler shift measurement can be used for the detection of gravitational waves, but the sensitivity of such measurement will be limited by laser frequency noise. Such laser frequency noise can be eliminated in a certain linear combination of the Doppler shift measurements; such linear combinations are called time-delay interferometer (TDI) variables [37, 38].

One such TDI variable is called the Michelson-like TDI variable X . It is defined as

$$X(t) = [\Delta\phi_3(t) + \Delta\phi_2(t - 2L)] - [\Delta\phi_2(t) + \Delta\phi_3(t - 2L)] \quad (41)$$

where $\Delta\phi_2(t)$ [$\Delta\phi_3(t)$] is the phase obtained by the laser along its round trip from SC1 to SC2 (SC3) at time t . This TDI- X variable measures the laser phase difference between two paths shown in Figure 5. Assuming an equal arm-length for simplicity, the X in the Fourier space is²

$$\tilde{X}(\omega) = \pm \frac{\omega_L}{\omega^2} e^{i\omega L} \int \frac{d^3k}{(2\pi)^3} e^{i\vec{k}\cdot\vec{x}_1} [i\vec{k} \cdot \vec{D}_X(\hat{n}_3, \hat{n}_2; L)] \tilde{\Psi}. \quad (42)$$

where

$$\vec{D}_X(\hat{n}_3, \hat{n}_2; L) = (1 - e^{2i\omega L})[\vec{D}(\hat{n}_3, L) - \vec{D}(\hat{n}_2, L)] = 2(1 - e^{2i\omega L})\vec{D}_{\text{Mich}}(\hat{n}_3, \hat{n}_2; L). \quad (43)$$

Here \hat{n}_2 (\hat{n}_3) is the unit vector from SC₁ and SC₂ (SC₃). The response vector \vec{D}_X is the same as that of the Michelson interferometer except for an overall factor of $2(1 - e^{2i\omega L})$. In the computations of the power spectrum, this additional factor leads to a common multiplication factor $16 \sin^2(\omega L)$, which will be ignored below.

The power spectrum due to ultralight dark matter fluctuation is

$$S_{\Delta L/L}^{\text{ULDM}}(\omega) = \frac{\bar{a}^2}{\omega^4 L^2} \tau \left[\sigma^4 A_{\text{Mich}}(\omega; \hat{n}_3, \hat{n}_2, L) + B_{\text{Mich}}(\omega; \hat{n}_3, \hat{n}_2, L) \right] \quad (44)$$

which is the same as the simple Michelson interferometer except that the two arms are not orthogonal to each other, $\hat{n}_2 \cdot \hat{n}_3 = 1/2 \neq 0$. The noise power spectrum is [39]

$$S_{\Delta L/L}(\omega) = \frac{1}{L^2} \left[S_N(\omega) + 2[1 + \cos^2(\omega L)] \frac{S_{\text{acc}}(\omega)}{\omega^4} \right]. \quad (45)$$

where $S_N(f)$ is the optical metrology noise power spectrum, and $S_{\text{acc}}(\omega)$ is the acceleration noise power spectrum. In this expression, the optical metrology and acceleration noise in each spacecraft are assumed to be identical, $S_{N_{ij}} = S_N$ and $S_{\text{acc},ij} = S_{\text{acc}}$. The noise spectrum and the ULDM spectrum will be compared later.

Similar to the Michelson interferometer, the response function can be obtained analytically in the isotropic and long wavelength limit. Assuming an equilateral configuration, we find

$$A_X \approx \frac{4}{3} \left(\frac{\bar{v}}{\sigma} \right)^6 e^{-(\bar{v}/\sigma)^2} \theta(\bar{v}^2) \left[\sin^4 \left(\frac{\omega L}{2} \right) + \frac{3}{8} (m\bar{v}L)^2 \cos(\omega L) \right] + (\omega \rightarrow -\omega) \quad (46)$$

$$B_X \approx \frac{32}{5\pi} |\bar{\omega}| K_1(|\bar{\omega}|) (m\sigma L)^2 \quad (47)$$

The behavior of the response function in the time-delay interferometer is the same as in the Michelson interferometer.

B. ULDM signal

Two distinct frequency components in the ULDM spectrum allow us to perform two different sets of analyses for the ultralight dark matter search. In what follows, we discuss how each frequency component of ultralight dark matter can be searched with matched filtering and cross-correlation of multiple detector outputs.

² In each spacecraft, two proof masses are loaded. We denote the position of proof masses loaded in SC_{*i*} as \vec{x}_i . We do not distinguish the difference in the position of two proof masses loaded in the same spacecraft. This is equivalent to assuming that the ULDM fluctuation perturbs two proof masses in the same spacecraft in the same way. This can be justified by noting that the wavelength of dark matter is always larger than the separation of proof masses in the same spacecraft.

1. Deterministic signal

The $\omega = 2m$ part of the spectrum represents the coherently oscillating ULDM signals. This is a deterministic signal in the sense that the signal form is known. For such deterministic signals, we can use the matched filter. Consider the detector output $d(t) = s(t) + n(t)$. By convoluting the detector output with the filter, $\int dt d(t)K(t)$, and choosing the filter $K(t)$ such that it maximally overlaps with the signal $s(t)$, one can add the signal coherently. The signal-to-noise ratio is

$$\frac{S}{N} = \left[\min(T, \sqrt{T\tau}) \int_{-\infty}^{\infty} df \frac{S_s(f)}{S_n(f)} \right]^{1/2} \quad (48)$$

where T is the total integration time scale and $\tau = 1/m\sigma^2$ is the coherence time scale of the deterministic signal. Here $S_s(f)$ is the power spectrum in differential arm length or strain unit from the ULDM fluctuations. The factor $\min(T, \sqrt{T\tau})$ denotes the gain in the signal-to-noise ratio in the coherent search, $S/N \sim \sqrt{T}$ when $T < \tau$ and the gain in the incoherent search, $S/N \sim T^{1/4}$ when $T > \tau$. This will be used to place an upper limit on dark matter density in the solar system. Note that the power spectrum in this expression is defined as a two-sided spectrum.

To proceed further, we note that the power spectrum of the coherently oscillating mode is narrowly peaked at $\omega = 2m$ with a width $\Delta\omega = m\sigma^2$. For the Michelson interferometry, the integral can be approximated as

$$\frac{S}{N} \approx \frac{\bar{a}\sigma^2}{2\pi^2 f_m^2 L} \left[\frac{\min(T, \sqrt{T\tau})}{S_{\Delta L/L}^{\text{one}}(f_m)} \right]^{\frac{1}{2}} \left[\tau \int_0^{\infty} df A_{\text{Mich}}(f) \right]^{\frac{1}{2}} \quad (49)$$

where $f_m = m/\pi$ and $S_{\Delta L/L}^{\text{one}}(f) = 2S_{\Delta L/L}(f)$ is the one-sided noise power spectrum. We have evaluated all the other factors in the integral at $f = f_m$ except for the exponential factor strongly peaked at $\omega = 2m$, assuming that they are smoothly distributed over $\Delta\omega \simeq m\sigma^2$. In the isotropic ($v_0/\sigma \ll 1$) and long-wavelength limit ($m\sigma L \ll 1$), one finds $\tau \int_0^{\infty} df A_{\text{Mich}} \simeq (8/\pi) \sin^4(f_m/2f_*)$ with $f_* = (2\pi L)^{-1}$. The above expression simplified to

$$\frac{S}{N} = \frac{2^{5/2}}{\sqrt{\pi}} \sin^2(f_m/2f_*) \left[\frac{\bar{a}\sigma^2}{(2\pi f_m)^2 L} \right] \left[\frac{\min(T, \sqrt{T\tau})}{S_{\Delta L/L}^{\text{one}}(f_m)} \right]^{\frac{1}{2}}. \quad (50)$$

The quantity in the first squared parenthesis is the typical displacement $\Delta L/L$ due to ULDM fluctuation during $\Delta t \sim 1/f_m$. Note that $\bar{a} = Gm_{\text{eff}}/\lambda^2$ and $m_{\text{eff}} = \pi^{3/2}\rho\lambda^3$. The above equation can be solved for ρ/ρ_0 with the local dark matter density $\rho_0 = 0.4 \text{ GeV}/\text{cm}^3$. For the interferometers with equilateral geometry, $\tau \int_0^{\infty} A_{\text{Mich}} \approx (4/\pi) \sin^4(f_m/2f_*)$. The additional factor of $1/2$ is because the two arms are not orthogonal to each other.

2. Stochastic signal

The low-frequency part of the ULDM spectrum behaves similarly to the stochastic gravitational wave background. To search for this part of the spectrum, we ideally need more than two detectors, which will allow us to cross-correlate the outputs in different detectors. If the separation of detectors is smaller than the wavelength of dark matter, the output at each detector is expected to be correlated, while the noise is expected to be uncorrelated. In this way, we can single out the ultralight dark matter signal in the output data stream of multiple detectors.

Consider two detector output $d_{1,2}(t) = s_{1,2}(t) + n_{1,2}(t)$ with the signal $s_{1,2}$ and the noise $n_{1,2}$. Then define the cross-correlated output Y as

$$Y = \int_{-T/2}^{T/2} dt \int_{-T/2}^{T/2} dt' d_1(t)d_2(t')Q(t-t') \simeq \int_{-\infty}^{\infty} df \tilde{d}_1(f)\tilde{d}_2^*(f)\tilde{Q}^*(f) \quad (51)$$

where $Q(t)$ is a real filter function. Suppose that the cross-correlation of signals at two detectors is $\langle \tilde{s}_1(f)\tilde{s}_2^*(f') \rangle = \delta(f-f')S_{12}(f)$. Using the optimal filter $\tilde{Q}(f) = S_{12}(f)/S_n^2(f)$ and assuming uncorrelated detector noise, one finds the signal-to-noise ratio as [40]

$$\frac{S}{N} = \left[T \int_{-\infty}^{\infty} df \frac{|S_{12}(f)|^2}{S_n^2(f)} \right]^{1/2}, \quad (52)$$

where T is the total integration time scale. In this way, the low-frequency part of the ultralight dark matter signal can be searched.

For cross-correlation, we are mostly interested in space-borne interferometers for the following reasons. For the cross-correlation to be relevant, two conditions need to be met: (i) the ultralight dark matter-induced signal must lie within the detector bandwidth, and (ii) the ultralight dark matter signals must be correlated in two detectors. Each interferometer has a range of frequencies to which the detector is sensitive. For the LIGO, the minimum frequency that LIGO is sensitive to is about $f_{\min} \sim 10$ Hz. On the other hand, two LIGO detectors, one at Hanford and the other at Livingston, are separated by $L_{\text{det}} \simeq 3000$ km. To guarantee that the ultralight dark matter signal is correlated over these two detectors, we require $L_{\text{det}} < (1/\Delta p) = (\sigma/\omega)$. This results in $\omega < 5 \times 10^{-2}$ Hz, which is more than two orders of magnitude smaller than the minimum detectable frequency in LIGO detectors. In other words, for the frequency range where the ultralight dark matter signals would be correlated over two LIGO detectors, LIGO detectors are not sensitive to ULDM signals due to a large seismic noise.

The situation in the space-borne interferometer is slightly different. For the sake of discussion, let us consider two coplanar LISA-like constellations. The minimum frequency of the LISA detector is $f_{\min} \sim 10^{-5}$ Hz. On the other hand, the detector separation is $L_{\text{det}} \sim L = 2.5 \times 10^6$ km or less. This translates into the condition $\omega < \sigma/L_{\text{det}} \simeq 10^{-4}$ Hz for ULDM signals to be correlated over two detectors. There is a range of frequencies where the signals are correlated over detectors, while the detector maintains its sensitivity to the ultralight dark matter signals. The same arguments hold for other types of proposed space-borne interferometers, such as μ Ares [25], a proposal using asteroids as GW detectors [26], and Big Bang Observatory (BBO) [41].

For this reason, we only consider space-borne interferometers. The cross-correlation of TDI-X variables is

$$S_{12}(f) = \frac{\bar{a}^2 \tau}{(2\pi f)^4 L^2} \mathcal{B}_{\text{cross}}. \quad (53)$$

The overlap function is

$$\begin{aligned} \mathcal{B}_{\text{cross}} = & \cos^2(2\pi f L) \mathcal{B}^{11'}(\vec{x}_{11'}) + \mathcal{B}^{33'}(\vec{x}_{33'}) + \mathcal{B}^{22'}(\vec{x}_{22'}) - \mathcal{B}^{23'}(\vec{x}_{23'}) - \mathcal{B}^{32'}(\vec{x}_{32'}) \\ & - \cos(2\pi f L) \left[\mathcal{B}^{31'}(\vec{x}_{31'}) + \mathcal{B}^{13'}(\vec{x}_{13'}) - \mathcal{B}^{21'}(\vec{x}_{21'}) - \mathcal{B}^{12'}(\vec{x}_{12'}) \right], \end{aligned} \quad (54)$$

where \vec{x}_i is the position of i -th spacecraft in the first constellation, $\hat{n}_{2,3} = (\vec{x}_{2,3} - \vec{x}_1)/L$, $\hat{n}_1 = (\vec{x}_3 - \vec{x}_2)/L$, $\vec{x}_{ij'} \equiv \vec{x}_i - \vec{x}_{j'}$, and $\mathcal{B}^{ab'} = \hat{n}_a^i \hat{n}_{b'}^j \mathcal{B}^{ij}$. The primed quantities are for the second constellation. We take $L = L'$ for simplicity. The signal-to-noise ratio is

$$\frac{S}{N} = \frac{\bar{a}^2}{(2\pi f_0)^4 L^2} \left[\frac{T}{(2\pi)^2} \int_{-\infty}^{\infty} df \left(\frac{f_0}{f} \right)^8 \frac{|\mathcal{B}_{\text{cross}}(f)|^2}{f_0^2 S_{\Delta L/L}^2(f)} \right]^{1/2}. \quad (55)$$

where $f_0 = \omega_0/2\pi = m\sigma^2/2\pi$. The prefactor is the squared value of the typical differential length change, $(\Delta L/L)^2$, over $\Delta t \sim 1/f_0$. The integral will be numerically solved.

C. Application

We apply the discussion in previous sections to the current and proposed gravitational wave interferometers.

1. LIGO

We take the sensitivity curve of LIGO O3 from Ref. [42]. The strain noise spectrum from ultralight dark matter can be found by using $S_{\Delta L/L}(f) = \text{sinc}^2(2\pi f L) S_h(f)$. For the LIGO with $f \lesssim 10^4$ Hz, $\text{sinc}(2\pi f L) \simeq 1$, we have ignored the additional $\text{sinc}^2(2\pi f L)$ factor. The arm length is $L_{\text{LIGO}} = 4$ km. As we have already estimated in the introduction, the ULDM-induced noise is by many orders of magnitude smaller than the instrumental noise. Still, it can provide an upper limit on the dark matter density in the solar system. For the search with a matched filter, we use (50) and rewrite it as

$$\frac{\rho}{\rho_0} \approx \frac{S}{N} \sqrt{\frac{\pi}{2}} \frac{1}{\text{sinc}^2(f_m/2f_*)} \left[\frac{(2\pi f_*)^2 L}{\bar{a}_0 \sigma^2} \right] \left[\frac{S_{\Delta L/L}^{\text{one}}(f_m)}{\min(T, \sqrt{T\tau})} \right]^{\frac{1}{2}} \quad (56)$$

where $\bar{a}_0 = Gm_{\text{eff},0}/\lambda^2$, $m_{\text{eff},0} = \pi^{3/2} \rho_0 \lambda^3$ with $\rho_0 = 0.4 \text{ GeV}/\text{cm}^3$, and $f_* = (2\pi L)^{-1} = 10^4$ Hz for LIGO. Note that for LIGO, we can also approximate $\text{sinc}^2(f_m/2f_*) \simeq 1$. For $T = 1 \text{ yr}$, $\sigma = 164 \text{ km}/\text{sec}$, and $S/N = 1$, the upper limit on the dark matter density ρ/ρ_0 is obtained and shown as a solid red line in Figure 2. Note that the above expression is valid in the long-wavelength limit $m\sigma L \ll 1$, which is satisfied not only in LIGO but also in all other ground-based interferometers.

2. Einstein Telescope

Einstein telescope is a proposed future gravitational wave detector based on a dual-recycled Michelson interferometer. The arm length is $L_{\text{ET}} = 10$ km. We assume an equilateral geometry for the Einstein telescope. The strain noise power spectrum is taken from [43]. Using the same expression (56) with $f_* = (2\pi L_{\text{ET}})^{-1} = 5 \times 10^3$ Hz, we show the upper limit on the density, ρ/ρ_0 , from Einstein Telescope with the blue solid line in Figure 2. We choose the same parameters: $T = 1$ yr, $\sigma = 164$ km/sec, and $S/N = 1$.

3. LISA

The noise source in LISA is conveniently divided into the collective optical metrology noise $S_N(f)$ and the single test-mass acceleration noise $S_{\text{acc}}(f)$. Each of them is given by [44]

$$S_N^{1/2}(f) = 10^{-11} \frac{\text{m}}{\sqrt{\text{Hz}}} \left[1 + \left(\frac{2\text{mHz}}{f} \right)^4 \right]^{1/2}, \quad (57)$$

$$S_{\text{acc}}^{1/2}(f) = 3 \times 10^{-15} \frac{\text{m s}^{-2}}{\sqrt{\text{Hz}}} \left[1 + \left(\frac{0.4\text{mHz}}{f} \right)^2 \right]^{\frac{1}{2}} \left[1 + \left(\frac{f}{8\text{mHz}} \right)^4 \right]^{\frac{1}{2}}. \quad (58)$$

LISA Pathfinder has reported differential acceleration noise of two test masses loaded in a single spacecraft, which is smaller than the LISA proposal requirement by a factor of few [45, 46]. For the matched filter search, we reuse (56) with an additional factor of $\sqrt{2}$, arising from the fact that LISA has an equilateral geometry and two arms are not orthogonal to each other. When recycling (56), we replace $\text{sinc}^2(f_m/2f_*) \rightarrow 1/[1 + (f_m/2f_*)^2]$ to show the envelope of the projection. The upper limit on the dark matter density ρ/ρ_0 with the same parameters is shown as a green solid line in Figure 2.

For the LISA, we also compare $S_{\Delta L/L}^{\text{ULDM}}(f)$ with the mission requirement $S_{\Delta L/L}(f)$. For the comparison, we compare two spectra in the GW strain unit. To convert to the strain noise power spectrum, we divided the power spectrum for the differential arm-length with the sky and polarization averaged detector response function $\mathcal{R}(f)$ [47],

$$\mathcal{R}(f) = \frac{3}{10(1 + 0.6(f/f_*)^2)}$$

with $f_* = (2\pi L_{\text{LISA}})^{-1} \simeq 19$ mHz. In the left panel of Figure 1, we show the mission requirement (red solid line) and S_n^{ULDM} with $m = 10^{-12}$ eV (cyan) and $m = 10^{-13}$ eV (orange). The ULDM-induced noise is several orders of magnitude smaller than the mission requirement, and therefore, it can safely be ignored for the purpose of gravitational wave detection.

The subdominant low-frequency ULDM signals might be probed if there are more than two detectors. Although the current LISA mission concept does not invoke more than two constellations [44], we assume two LISA-like interferometers and investigate the reach of such configuration for the ULDM search as an exercise. Note that other space-borne interferometers, such as Taiji and TianQin, would allow the cross-correlation searches [30]. For the cross-correlation, the position of the spacecraft needs to be specified. In the heliocentric ecliptic coordinate, their position is [48]

$$x = a \cos \alpha + ae[\sin \alpha \cos \alpha \sin \beta - (1 + \sin^2 \alpha) \cos \beta] \quad (59)$$

$$y = a \sin \alpha + ae[\sin \alpha \cos \alpha \cos \beta - (1 + \cos^2 \alpha) \sin \beta] \quad (60)$$

$$z = \sqrt{3}ae \cos(\alpha - \beta) \quad (61)$$

where $a \approx \text{AU}$ is the semi-major axis, e is eccentricity, $\alpha = \omega t + \kappa$, and $\beta = 2n\pi/3 + \lambda$ with $n = 0, 1, 2$. Here α is the orbital phase of the guiding center. Note that the arm length is given by $L = 2\sqrt{3}\epsilon R$; for $R = \text{AU}$ and $L_{\text{LISA}} = 2.5 \times 10^6$ km, the eccentricity is $\epsilon = 4.8 \times 10^{-3}$. The position of spacecraft in the second constellation is given by the same expression but with a prime (κ' , λ' , and so on).

Rewriting (55) in terms of ρ/ρ_0 , we find

$$\frac{\rho}{\rho_0} = \frac{1}{2^{3/4}} \left(\frac{S}{N} \right)^{\frac{1}{2}} \left[\frac{(2\pi f_0)^2 L}{\bar{a}_0} \right] \left[\frac{T}{(2\pi)^2} \int_0^\infty df \left(\frac{f_0}{f} \right)^8 \frac{|\mathcal{B}_{\text{cross}}|^2}{f_0^2 |S_{\Delta L/L}^{\text{one}}(f)|^2} \right]^{-\frac{1}{4}}. \quad (62)$$

Using the halo dark matter parameters, $\sigma = 164$ km/sec and $\rho_0 = 0.4 \text{ GeV/cm}^3$, and assuming $\Delta\kappa = \kappa' - \kappa = 0$ (co-planar configuration), $\Delta\lambda = \lambda' - \lambda = \pi/2$, and $T = 5$ yr, we find the reach of two LISA-like detectors as a dashed

green line in Figure 2. For the frequency range, we use $f_{\min} = 10^{-5}$ Hz and $f_{\max} = 1$ Hz. We have included a galactic confusion noise, assuming $T = 4$ yr of operation [49].

4. μ Ares

We also consider the μ Ares proposal [25] for the ultralight dark matter search. The proposed concept is similar to LISA in the sense that it consists of three spacecraft, and it operates as a time-delay interferometer. The configuration of satellites is heliocentric, while the arm-length is $L = 400$ M km. For the matched filter and cross-correlation analysis, we take the strain noise power spectrum in [25], including astrophysical foreground. The upper limit on the dark matter density ρ/ρ_0 with matched filtering is shown as a purple line in Figure 2.

We also compare the ultralight dark matter-induced noise with the required noise level for the proposed mission concept. The proposal requires $S_{\text{acc}}^{1/2}(f) = 10^{-15} \text{ m s}^{-2}/\sqrt{\text{Hz}}$, and $S_N^{1/2}(f) = 50 \text{ pm}/\sqrt{\text{Hz}}$. The result is shown on the right panel of Figure 1 for $m = 10^{-12}$ – 10^{-15} eV. Note that the noise curve in this figure is obtained by using (45) with the proposal requirements, but without any astrophysical foregrounds. Note also that, for $f \lesssim$ a few $\times 10^{-7}$ Hz, the gravity gradient noise from asteroids could dominate the total noise spectrum [27].

For the cross-correlation analysis, we specify the position of each spacecraft in the heliocentric ecliptic coordinate as

$$\vec{x}_n = R\left(\cos[\phi + 2\pi(n-1)/3], \sin[\phi + 2\pi(n-1)/3], 0\right) \quad (63)$$

where $n = 1, 2, 3$ and ϕ is the orbital phase of the interferometer. We assume another of such constellations lying on the same plane (co-planar configuration), with the relative phase with respect to the first constellation by $\Delta\phi$. Using (62), we find the projected sensitivity of ρ/ρ_0 of the cross-correlation search in μ Ares as a purple dashed line in Figure 2. We use $f_{\min} = 4 \times 10^{-7}$ Hz, $f_{\max} = 10^{-1}$ Hz, and $\Delta\phi = \pi/2$.

5. Big Bang Observatory

The configuration of the Big Bang Observatory is similar to the LISA, except for a smaller arm-length, $L_{\text{BBO}} = 5 \times 10^7$ m. The instrument parameters are [50]

$$S_N^{1/2} = 1.4 \times 10^{-17} \text{ m}/\sqrt{\text{Hz}}, \quad (64)$$

$$S_{\text{acc}}^{1/2} = 3 \times 10^{-17} \text{ m s}^{-2}/\sqrt{\text{Hz}}. \quad (65)$$

The cross-correlation search is identical to the one in LISA, except for this arm-length difference and different instrumental parameters. The matched filter and cross-correlation search (using two co-planar constellations) yields the upper limit on ρ/ρ_0 , represented by the (dashed) brown lines in Figure 2. For the analysis, we use $f_{\min} = 10^{-4}$ Hz, $f_{\max} = 10^2$ Hz, and $\Delta\lambda = \pi$. We have included the same galactic confusion noise as in the case of LISA while assuming the other astrophysical foreground around $\sim \mathcal{O}(0.1)$ Hz from neutron star binaries can be fully resolved [51].

IV. DISCUSSION

We discuss now some of the ignored effects in the main discussion and some of the other implications of our results.

In the main discussion, we have ignored the mean acceleration on the test masses due to ULDm; we have considered only its variance. The mean acceleration is nothing but the dynamical friction, and it is present as long as $\vec{v}_0 \neq 0$ in the rest frame of the detector. One may directly compute the dynamical friction from the expression (19). The dynamical friction for the ultralight dark matter has already been obtained in [52], where it is given by

$$\langle a^i \rangle = \hat{v}_0^i \frac{8\pi G^2 \rho m_{\text{eff}} \ln \Lambda}{\sigma^2} \left[G\left(\frac{v_0}{\sigma}\right) + \frac{m_t}{2m_{\text{eff}}} G\left(\frac{v_0}{\sqrt{2}\sigma}\right) \right] \quad (66)$$

Here $G(X) = 1/(2X^2)[\text{erf}(X) - (2X/\sqrt{\pi})e^{-X^2}]$, m_t is the mass of the test body, and $\ln \Lambda$ is the Coulomb logarithm factor arising due to the long-range nature of gravitational force. For the halo dark matter with $\rho_0 = 0.4 \text{ GeV}/\text{cm}^3$ and $m = 10^{-22}$ eV, this dynamical friction force is causing $\Delta x \sim \mathcal{O}(1)$ meter of drift of constellation over a year, which is much smaller than the expected unavoidable change of arm-length of LISA, $\Delta x \sim \mathcal{O}(10^4\text{--}10^5)$ km, due to the

orbital dynamics [44]. In addition, the dynamical friction force acts on each spacecraft in the same way, and therefore, we do not expect that it changes the arm length itself. For these reasons, we do not expect that the dynamical friction is relevant for the discussion of the ULDM-induced signals in the interferometers.

We have found that some of the future gravitational wave interferometers could potentially probe $\rho/\rho_0 \sim \mathcal{O}(10^2)$ where $\rho_0 = 0.4 \text{ GeV/cm}^3$ is the local dark matter density. Since we have projected the sensitivity of interferometers in units of ρ_0 and this local dark matter density is one of the key input parameters for all terrestrial dark matter detectors, it is worthwhile to discuss how this value $\rho_0 \sim \mathcal{O}(0.1) \text{ GeV/cm}^3$ is obtained. The current measurement of local dark matter is usually performed over a much larger spatial scale. For instance, even the very local measurements of the dark matter density select stellar tracers within $\mathcal{O}(10^2) \text{ pc}$ around the solar system, and therefore, the inferred value of dark matter density is an average value over that spatial volume, $V \sim [\mathcal{O}(10^2) \text{ pc}]^3$ [28, 29]. When it comes to the measurement within the solar system, the dark matter density is poorly constrained. Measurement using the planetary ephemerides places an upper limit on the dark matter density in the solar system as $\rho/\rho_0 \lesssim 10^4$ [53], while the measurements of lunar laser ranging and LAGEOS geodetic satellite place an upper limit on the dark matter density between the Moon and the satellite's orbital radius as $\rho/\rho_0 \lesssim 10^{11}$ [54].

Furthermore, a large density fluctuation might just arise statistically in the ultralight dark matter halo. For the density of the field, ρ_ϕ , its underlying distribution is given by the exponential distribution, $p(\rho_\phi)d\rho_\phi = [\exp(-\rho_\phi/\rho_0)/\rho_0]d\rho_\phi$ (see Appendix C). Given that the correlation of density field exponentially drops over $L \gtrsim 1/m\sigma$ [52], we may consider the density fluctuation ρ_ϕ over wavelength-sized patches as statistically independent random variables. The probability of finding a patch with $\rho_\phi > c\rho_0$ is then given by

$$P(\rho_\phi > c\rho_0) = \int_{c\rho_0}^{\infty} p(\rho_\phi) = e^{-c}.$$

On the other hand, the number of statistically independent patches over the volume V is $N \sim V/\lambda^3$. For $m = 10^{-15} \text{ eV}$, the wavelength is about AU scale, and the number of patches over $V = (10 \text{ kpc})^3$ volume is $N = V/\lambda^3 = (10 \text{ kpc}/\text{AU})^3 \sim 10^{28}$. For $c = 60$, one finds $P(\rho_\phi > 60\rho_0) = e^{-60} \simeq 10^{-26}$. This would mean that there might be several hundreds of AU-sized patches within 10 kpc volume with $\rho \gtrsim 60\rho_0$.

We have only considered cross-correlation searches for space-borne interferometers. The reason that it was not suitable for the ground-based interferometers, especially for the current advanced LIGO, was that the detector separation is too large for the ultralight dark matter signals to be correlated for the relevant frequency range of the detector. However, in the initial LIGO phase, two detectors at Hanford, with 4 km and 2 km arms, were co-located and co-aligned, and therefore, it is in principle possible to use the result of two Hanford detectors in the initial LIGO phase for the cross-correlation search as demonstrated in [55, 56] for the stochastic gravitational waves. Since the detectors are co-located, environmental noises are correlated, and this correlated noise must be carefully accounted for in the analysis.

For the low-frequency ULDM signals, we have considered the cross-correlation, which requires more than two detectors. One may still be able to search for these low-frequency ULDM signals with a single detector with the help of a null data stream. A null data stream is the output of the detector where the expected signal, either GWs or ULDM, is expected to be suppressed, allowing a way to calibrate the instrumental noises. For the time-delay interferometers, like LISA, a symmetrized Sagnac channel is shown to be insensitive to the gravitational wave signals at low frequencies, $f < f_* = (2\pi L)^{-1}$, which could, at least partially, provide a way to distinguish for stochastic gravitational wave backgrounds from other noise sources at such low frequencies [57–59]. Similarly to the stochastic gravitational wave backgrounds, ultralight dark matter signal is strongly suppressed in the symmetrized Sagnac channel as $\propto (m\sigma L)^4$ for $m\sigma L < 1$, and therefore, using such null data stream might provide a way to search for ULDM at sufficiently small masses with the help of additional information such as annual modulations of the ULDM signal.

V. CONCLUSION

We have investigated how the density fluctuations of ultralight dark matter interact with interferometers, designed for the detection of gravity waves. We provide a systematic way to compute the ULDM spectrum in any gravitational wave interferometers. We show that the ultralight dark matter-induced noise is most significant when the arm-length is large, such as LISA or other proposals with an astronomical size of arm-length, and that, in all cases, we consider, the ultralight dark matter effects are subdominant compared to other noise sources, e.g. interferometric read-out noise and acceleration noise. Then we consider if such interferometers can be used to place an upper bound on the dark matter density in the solar system, and find that, under certain assumptions, $\rho/\rho_0 \sim \mathcal{O}(10^2)$ might be probed with future gravitational wave interferometers with its arm-length close to astronomical unit.

We note that the current local dark matter density measurement, $\rho_0 = 0.4 \text{ GeV}/\text{cm}^3$, is performed on a much larger scale, e.g. $\gtrsim \mathcal{O}(100) \text{ pc}$, and that the constraints on dark matter abundance in the solar system from planetary ephemerides and laser ranging experiments are several orders of magnitude larger than ρ_0 . Especially in the light of a situation where there is no direct and gravitational detection of dark matter in the solar system, these interferometric approaches will provide an interesting way to probe ultralight dark matter only through gravitational interaction. In addition, it has been recently proposed that the ultralight dark matter density in the solar system might be larger than the local dark matter density through certain capture processes [60–62]. Our interferometric search for ultralight dark matter in the solar system is expected to provide an interesting probe for such possibilities.

Our analysis can be straightforwardly generalized to pulsar timing array (PTA) observations. Coherent ULDM signals in PTA observations were already explored by Khmelnitsky and Rubakov [63], whose results are reproduced in Appendix D with the formalism discussed in this work. Low-frequency stochastic fluctuations of ULDM in the context of pulsar timing measurements, however, have not been explored. As the distance between the Earth and pulsars is on a kiloparsec scale, and the pulsar timing analyses involve a cross-correlation of timing residuals of pulsars with different sky locations, PTAs offer another interesting probe for stochastic ULDM density fluctuations. In future work, we will investigate how these stochastic ULDM signals affect pulsar timing measurements and if one can probe ULDM density within the solar system with PTA observations [64].

ACKNOWLEDGMENTS

We would like to thank Julián Rey and Nicholas Rodd for useful conversations. We especially thank Alessandro Lenoci for the initial collaboration. We also thank Thomas Konstandin, Germano Nardini, and Mauro Pieroni for their useful comments and suggestions on the manuscript. This work is supported by the Deutsche Forschungsgemeinschaft under Germany’s Excellence Strategy - EXC 2121 Quantum Universe - 390833306.

Appendix A: Power spectrum

We provide a detailed computation of the low-frequency part of the power spectrum $S_{\nabla\Psi}^{ij}(\omega, \vec{L})$. To prepare an explicit computation, we derive the integral expression of the power spectrum (25) in the non-relativistic limit:

$$\begin{aligned} S_{\nabla\Psi}^{ij}(\omega, \vec{L}) = & 32\pi^3 G^2 \int d^3 v_c \int d^3 v_d f(\vec{v}_c + \vec{v}_d) f(\vec{v}_c - \vec{v}_d) \\ & \times \left[v_c^i v_c^j \left(\delta(\omega - \omega_1 - \omega_2) e^{2im\vec{v}_c \cdot \vec{L}} + \delta(\omega + \omega_1 + \omega_2) e^{-2im\vec{v}_c \cdot \vec{L}} \right) \right. \\ & \left. + \frac{v_d^i v_d^j}{v_d^4} \left(\delta(\omega - \omega_1 + \omega_2) e^{2im\vec{v}_d \cdot \vec{L}} + \delta(\omega + \omega_1 - \omega_2) e^{-2im\vec{v}_d \cdot \vec{L}} \right) \right] \end{aligned} \quad (\text{A1})$$

where we have introduced new integration variables \vec{v}_c and \vec{v}_d , defined as

$$\vec{v}_c = \frac{1}{2}(\vec{v}_1 + \vec{v}_2), \quad \vec{v}_d = \frac{1}{2}(\vec{v}_1 - \vec{v}_2).$$

The two terms in the first line are related by the complex conjugate with $\omega \rightarrow -\omega$. The two terms in the last line are the same under the exchange of the integration variable $\vec{v}_1 \leftrightarrow \vec{v}_2$. The first two terms represent the spectrum at $\omega = \pm 2m$, denoted by $A^{ij}(\omega, \vec{L})$ in the main text, and the last two terms represent the low-frequency part, denoted by $B^{ij}(\omega, \vec{L})$. Since the computation of $\omega = \pm 2m$ mode is straightforward, only the computation of B^{ij} will be given below.

The relevant part of the power spectrum is

$$S_{\nabla\Psi}^{ij}(\omega, \vec{L}) = \frac{32\pi^3 G^2}{m} \int d^3 v_c \int d^3 v_d f(\vec{v}_c + \vec{v}_d) f(\vec{v}_c - \vec{v}_d) \frac{v_d^i v_d^j}{v_d^4} \delta\left(\vec{v}_c \cdot \vec{v}_d - \frac{\omega}{2m}\right) e^{2im\vec{v}_d \cdot \vec{L}} \quad (\text{A2})$$

where we have used the symmetry of integrand under the exchange of integration variable $v_1 \leftrightarrow v_2$ in (A1) and take the non-relativistic limit for the δ -function.³ Using the normal distribution

$$f(\vec{v}) = \frac{(\rho_0/m)}{(2\pi\sigma^2)^3} \exp\left[-\frac{(\vec{v} - \vec{v}_0)^2}{2\sigma^2}\right],$$

³ In the case of $\vec{L} = 0$ and $\omega \rightarrow 0$ the above power spectrum is nothing but the second diffusion coefficient $D[\Delta v^i(T)\Delta v^j(T)] = \langle \Delta v^i(T)\Delta v^j(T) \rangle / T$ of the test mass with the change of velocity $\Delta v^i(T)$ over the time T . Compare the expression with (54) in Bar-Or et al [52].

we find

$$\begin{aligned}
S_{\nabla\Psi}^{ij}(\omega, \vec{L}) &= \frac{4(G\rho_0)^2}{m^3\sigma^6} \int d^3v_c \int d^3v_d \exp \left[-\frac{(\vec{v}_c - \vec{v}_0)^2}{\sigma^2} - \frac{v_d^2}{\sigma^2} \right] \frac{v_d^i v_d^j}{v_d^4} \delta \left(\vec{v}_c \cdot \vec{v}_d - \frac{\omega}{2m} \right) e^{2im\vec{v}_d \cdot \vec{L}} \\
&= \frac{4(G\rho_0)^2}{m^3\sigma^4} \int d^3v_c \int d^3v_d e^{-(\vec{v}_c - \vec{v}_0/\sigma)^2} e^{-v_d^2} \frac{v_d^i v_d^j}{v_d^4} \delta \left(\vec{v}_c \cdot \vec{v}_d - \frac{\bar{\omega}}{2} \right) e^{2i\vec{v}_d \cdot \vec{L}_\lambda} \\
&= -\frac{(G\rho_0)^2}{m^3\sigma^4} \frac{\partial^2}{\partial L_\lambda^i \partial L_\lambda^j} \int d^3v_c \int d^3v_d e^{-(\vec{v}_c - \vec{v}_0/\sigma)^2} e^{-v_d^2} \frac{1}{v_d^4} \delta \left(\vec{v}_c \cdot \vec{v}_d - \frac{\bar{\omega}}{2} \right) e^{2i\vec{v}_d \cdot \vec{L}_\lambda} \tag{A3}
\end{aligned}$$

where in the second line we have changed the integration variables $\vec{v}_{c,d} \rightarrow \vec{v}_{c,d}\sigma$, and defined $\vec{L}_\lambda = m\sigma\vec{L}$. In the last line, the vector v_d^i in the integrand is replaced with the derivative with respect to \vec{L}_λ .

To proceed further, we use the integral representation of δ -function: $\delta(x) = \int (ds/2\pi) e^{-ixs}$. We then perform the \vec{v}_c integral, and then the \hat{v}_d integral. After some manipulation, we find

$$S_{\nabla\Psi}^{ij}(\omega, \vec{L}) = -4\pi^{3/2} \frac{(G\rho_0)^2}{m^3\sigma^4} \frac{\partial^2}{\partial L_\lambda^i \partial L_\lambda^j} \int_{-\infty}^{\infty} ds e^{-is\bar{\omega}} \sqrt{1+s^2} \int_0^{\infty} \frac{e^{-y^2}}{y^2} \text{sinc}(2yY) \tag{A4}$$

where $\vec{Y} = (1+s^2)^{-1/2}(s\vec{v}_0/\sigma + \vec{L}_\lambda)$. The y integral is divergent. The divergence can be regulated by $\text{sinc}(2yY) \rightarrow \text{sinc}(2yY) - 1$. The additional -1 term would not contribute to the final result as it does not depend on L_λ . Using this regularization, we obtain

$$\begin{aligned}
S_{\nabla\Psi}^{ij}(\omega, \vec{L}) &= (\bar{a}^2\tau) \left[\frac{2}{\sqrt{\pi}} \int_{-\infty}^{\infty} \frac{e^{-is\bar{\omega}}}{\sqrt{1+s^2}} \left(\delta^{ij} \frac{\text{erf}(Y) - G(Y)}{Y} + Y^i Y^j \frac{3G(Y) - \text{erf}(Y)}{Y^3} \right) \right] \\
&\equiv (\bar{a}^2\tau) B^{ij}(\omega, \vec{L}). \tag{A5}
\end{aligned}$$

This reproduces the result used in the main text.

Appendix B: Induced phase

In this Appendix, we discuss the approximation for the phase (34). We begin with

$$\Delta\phi(t) = 2\omega_L(\delta t + \delta L) \tag{B1}$$

where the time delay δt and the arm-length fluctuation δL are

$$\delta L = +\frac{1}{2} \hat{x} \cdot \left[(\delta\vec{x}_1(t-L) - \delta\vec{x}_0(t-2L)) + (\delta\vec{x}_1(t-L) - \delta\vec{x}_0(t)) \right], \tag{B2}$$

$$\delta t = -\frac{1}{2} \left[\int_{t-L}^t dt' + \int_{t-2L}^{t-L} dt' \right] [\Psi(t', \vec{x}(t')) + \Phi(t', \vec{x}(t'))]. \tag{B3}$$

In the Fourier space, each of them is

$$\widetilde{\delta L}(\omega) = e^{i\omega L} \hat{x} \cdot [\delta\vec{x}_1(\omega) - \cos(\omega L)\delta\vec{x}_0(\omega)] = \frac{e^{i\omega L}}{\omega^2} \int \frac{d^3k}{(2\pi)^3} e^{i\vec{k} \cdot \vec{x}_0} \left[e^{i\vec{k} \cdot \hat{n}L} - \cos(\omega L) \right] (i\vec{k} \cdot \hat{n}) \tilde{\Phi} \tag{B4}$$

$$\widetilde{\delta t}(\omega) = -e^{i\omega L} \int \frac{d^3k}{(2\pi)^3} e^{i\vec{k} \cdot \vec{x}_0} \left[\frac{(e^{i\vec{k} \cdot \hat{n}L} - \cos\omega L)(i\vec{k} \cdot \hat{n}) + \omega \sin\omega L}{\omega^2 - (\vec{k} \cdot \hat{n})^2} \right] (\tilde{\Phi} + \tilde{\Psi}) \tag{B5}$$

where we have used $\delta\vec{x}_i(\omega) = -(1/\omega)^2 \int [d^3k/(2\pi)^3] e^{i\vec{k} \cdot \vec{x}_i} \tilde{a}(\omega, \vec{k})$ and $\tilde{a}(k) = -i\vec{k}\tilde{\Phi}(k)$. Here $\hat{n} = (\vec{x}_1 - \vec{x}_0)/L$. The phase in the frequency space is

$$\widetilde{\Delta\phi}(\omega) = 2e^{i\omega L} \omega_L \int \frac{d^3k}{(2\pi)^3} e^{i\vec{k} \cdot \vec{x}_0} \left[\frac{(e^{i\vec{k} \cdot \hat{n}L} - \cos\omega L)(i\vec{k} \cdot \hat{n})}{\omega^2} \tilde{\Phi} - \frac{(e^{i\vec{k} \cdot \hat{n}L} - \cos\omega L)(i\vec{k} \cdot \hat{n}) + \omega \sin\omega L}{\omega^2 - (\vec{k} \cdot \hat{n})^2} (\tilde{\Phi} + \tilde{\Psi}) \right]. \tag{B6}$$

To simplify this expression, let us consider the power spectrum for the metric perturbation in the non-relativistic limit. They are given as

$$P_{\Psi}(k) = \frac{(4\pi Gm)^2}{2k^4} (2\pi)^4 \int d^3v_1 d^3v_2 f_1 f_2 \left[v_c^4 \delta^{(4)}(k - p_1 - p_2) + \delta^{(4)}(k - p_1 + p_2) \right] + (k \rightarrow -k) \quad (\text{B7})$$

$$P_{\Phi}(k) = \frac{(4\pi Gm)^2}{2k^4} (2\pi)^4 \int d^3v_1 d^3v_2 f_1 f_2 \left[(v_c^2 + v_d^2 - 3(\hat{v}_c \cdot \vec{v}_d)^2) \delta^{(4)}(k - k_1 - k_2) + \delta^{(4)}(k - k_1 + k_2) \right] + (k \rightarrow -k) \quad (\text{B8})$$

where $f_i = f(\vec{v}_i)$ is the velocity distribution. In both cases, the $\omega = 2m$ mode is velocity suppressed, while $\omega < m\sigma^2$ does not have such velocity suppression.

Let us first consider $\omega < m\sigma^2$ modes. In this case, $\tilde{\Phi} = \tilde{\Psi}$ and $\omega/k \sim \sigma \ll 1$. Therefore, the time delay contribution is suppressed by $(\omega/k)^2 \sim \sigma^2$ compared to the test mass acceleration. Hence, the phase is approximated as

$$\tilde{\Delta}\phi(\omega) = e^{i\omega L} \frac{\omega L}{\omega^2} \int \frac{d^3k}{(2\pi)^3} e^{i\vec{k} \cdot \vec{x}_0} (i\vec{k} \cdot \vec{D}) \tilde{\Psi} \quad (\text{B9})$$

with $\vec{D}(\hat{n}, L) = \hat{n}(e^{i\vec{k} \cdot \hat{n}L} - \cos \omega L)$.

Now consider $\omega = 2m$. In this case, $\omega/k \sim 1/\sigma \gg 1$. The phase is approximated as

$$\begin{aligned} \tilde{\Delta}\phi(\omega) &\approx -2e^{i\omega L} \frac{\omega L}{\omega^2} \int \frac{d^3k}{(2\pi)^3} e^{i\vec{k} \cdot \vec{x}_0} \left[(e^{i\vec{k} \cdot \hat{n}L} - \cos \omega L) (i\vec{k} \cdot \hat{n}) \tilde{\Psi} + \omega \sin \omega L \left(1 + \frac{(\vec{k} \cdot \hat{n})^2}{\omega^2} \right) (\tilde{\Phi} + \tilde{\Psi}) \right] \\ &= -2e^{i\omega L} \frac{\omega L}{\omega^2} \int \frac{d^3k}{(2\pi)^3} e^{i\vec{k} \cdot \vec{x}_0} \left[(e^{i\vec{k} \cdot \hat{n}L} - \cos \omega L - i(\vec{k} \cdot \hat{n}L) \text{sinc} \omega L) (i\vec{k} \cdot \hat{n}) \tilde{\Psi} + \text{sinc} \omega L (\vec{k} \cdot \hat{n})^2 L \tilde{\Phi} \right] \end{aligned} \quad (\text{B10})$$

In the second line, we neglect the $\omega \sin(\omega L)(\tilde{\Phi} + \tilde{\Psi})$ term. Interferometers are always sensitive to the phase difference, and since this term does not have any dependence on the direction of light propagation, it cancels out in the final interferometer observables. For $\omega L \gtrsim 1$ and for $kL < (\omega L)^2 < 1$, the terms proportional to $(\vec{k} \cdot \hat{n})^2$ are negligible, and thus, the phase is approximated as

$$\tilde{\Delta}\phi(\omega) \approx -e^{i\omega L} \frac{\omega L}{\omega^2} \int \frac{d^3k}{(2\pi)^3} e^{i\vec{k} \cdot \vec{x}_0} (i\vec{k} \cdot \vec{D}) \tilde{\Psi} \quad (\text{B11})$$

For $(\omega L)^2 < kL$, the dominant term is the one proportional to $\tilde{\Phi}$, so a more correct approximation would be obtained by replacing $\tilde{\Psi} \rightarrow -\tilde{\Phi}$ from (B11). Since $\tilde{\Phi} \sim \tilde{\Psi}$ up to an order one numerical factor, the above expression still provides a reasonable approximation even in this limit. In summary, the phase in both cases can be approximated as

$$\tilde{\Delta}\phi(\omega) = \pm e^{i\omega L} \frac{\omega L}{\omega^2} \int \frac{d^3k}{(2\pi)^3} e^{i\vec{k} \cdot \vec{x}_0} (i\vec{k} \cdot \vec{D}) \tilde{\Psi}. \quad (\text{B12})$$

Appendix C: Density fluctuation

We compute the statistical properties of (mass) density fluctuation. In the non-relativistic limit, the density field becomes

$$\hat{\rho}_\phi \approx \sum_{i,j} \frac{m}{V} a_i^\dagger a_j e^{i(k_i - k_j) \cdot x}, \quad (\text{C1})$$

where we have ignored quantum fluctuations arising from the commutation relation. From the above expression with the quasi-probability distribution (5), moments of the density field can be computed as

$$\langle \rho_\phi^n \rangle = n! \rho_0^n. \quad (\text{C2})$$

They are identical to those random variables under the exponential distribution. Therefore, we find

$$p(\rho_\phi) d\rho_\phi = \frac{e^{-\rho_\phi/\rho_0}}{\rho_0} d\rho_\phi \quad (\text{C3})$$

with $\rho_\phi \in [0, \infty)$. The density fluctuation in the ultralight dark matter halo is larger than the particle dark matter halo since particle dark matter density follows the Poisson statistics.

Appendix D: Coherent signals in pulsar timing array

The pulsar timing array (PTA) measures the time-of-arrival of pulses from pulsars. Similar to the previous discussion, the time-of-arrival is affected by ULDM fluctuations through Shapiro time delay, Doppler effect, and Einstein delay. An arrival time of a pulse is given by

$$\tau \simeq \tau_{\text{em}} + L + \delta\tau_1 + \delta\tau_2 + \delta\tau_3 \quad (\text{D1})$$

where τ is the proper time of an observer at the observing time, τ_{em} is the proper time at the pulsar at the emission time, L is the nominal distance between the pulsar and the earth, and

$$\delta\tau_1(t) = -\hat{n} \cdot [\delta\vec{x}_{\oplus}(t) - \delta\vec{x}_{\text{psr}}(t - L)], \quad (\text{D2})$$

$$\delta\tau_2(t) = -\int_{t-L}^t dt' [\Phi(t', \vec{x}(t')) + \Psi(t', \vec{x}(t'))], \quad (\text{D3})$$

$$\delta\tau_3(t) = \int^t dt' [\Phi(t', \vec{x}_{\oplus}) - \Phi(t' - L, \vec{x}_{\text{psr}})]. \quad (\text{D4})$$

Here $\delta\tau_1$ is due to the change in distance between earth-pulsar system similar to (B2) (Doppler effect), $\delta\tau_2$ is the Shapiro time delay similar to (B3), and $\delta\tau_3$ is due to the conversion between the proper time τ and the coordinate time t (Einstein delay). Note that \hat{n} is the unit vector pointing to the pulsar.

The next pulse arrives at τ' ,

$$\tau' \simeq \tau_{\text{em}} + L + T + \delta\tau_1(t + T) + \delta\tau_2(t + T) + \delta\tau_3(t + T) \quad (\text{D5})$$

where T is the rotational period of the pulsar. The difference in time between the two arrival times is

$$\tau' - \tau = T + \Delta T \quad (\text{D6})$$

where the time delay ΔT is

$$\Delta T = \sum_{i=1}^3 [\delta\tau_i(t + L) - \delta\tau_i(t)]. \quad (\text{D7})$$

The rotational period of pulsars used in PTA analysis is a few milliseconds, $T \sim \mathcal{O}(10^{-3})$ sec, while the coherent signal we are looking for has a frequency of a few nano Hz, $f \sim \text{nHz}$. This suggests that the fluctuations due to ULDM do not significantly change over the rotational time scale T . In the limit $fT \ll 1$, the time delay can be simplified as

$$\begin{aligned} \frac{\Delta T}{T}(t) &= -\hat{n} \cdot [\delta\vec{v}_{\oplus}(t) - \delta\vec{v}_{\text{psr}}(t - L)] - \Psi(t, \vec{x}_{\oplus}) + \Psi(t - L, \vec{x}_{\text{psr}}) \\ &+ \int_{t-L}^t dt' \hat{n} \cdot \nabla [\Phi(t', \vec{x}(t')) + \Psi(t', \vec{x}(t'))]. \end{aligned} \quad (\text{D8})$$

This (approximate) time delay expression coincides with the redshift of the photon up to the sign [63, 65]. Note that the Doppler shift was ignored in the work of Khmel'nitsky and Rubakov [63].

The timing residual is computed by integrating the above time delay over time:

$$R(t) = \int_0^t dt' \frac{\Delta T}{T}(t'). \quad (\text{D9})$$

For the coherent oscillation at $\omega = 2m$, the largest contribution to the timing residual arises from $-\Psi(t, \vec{x}_{\oplus}) + \Psi(t - L, \vec{x}_{\text{psr}})$ part in the time delay. In particular, one finds

$$\langle R(t)^2 \rangle \approx \int \frac{d^4 k}{(2\pi)^4} \frac{2}{\omega^4} P_{\Psi}(k) \quad (\text{D10})$$

where we have ignored fast-oscillating terms. The power spectrum is given by $P_{\Psi}(k) = [(4\pi G)^2/k^4]P_{\delta\rho}(k)$, where the density fluctuation power spectrum around $\omega \simeq 2m$ is

$$P_{\delta\rho}(k) = \frac{2\pi^2 \rho^2}{m^4 \sigma^5} \left[\left(\frac{v_k^4}{16} \left(\frac{\bar{v}^2}{\sigma^2} - \frac{v_k^2}{4\sigma^2} \right)^{1/2} e^{-\bar{v}^2/\sigma^2} + (\omega \rightarrow -\omega) \right) + \frac{\sigma}{v_k} \exp \left(-\frac{v_k^2}{4\sigma^2} - \frac{\sigma^2 |\bar{\omega}|^2}{v_k^2} \right) \right] \quad (\text{D11})$$

The first term in the squared parenthesis represents the coherently oscillating mode at $\omega = 2m$, while the second term represents the stochastic modes. This expression assumes $v_0 = 0$. Note also that $\bar{v}^2(\omega) = (\omega/m - 2)$, $v_k = k/m$, and $\bar{\omega} = \omega/m\sigma^2$. An explicit computation with the coherently oscillating modes reveals

$$\langle R(t)^2 \rangle \approx \frac{\pi^2 (G\rho)^2}{2m^6} \quad (\text{D12})$$

which agrees with the result in Ref. [63]. While our main discussion focuses on computing the differential phase induced by ULDM in an interferometric setup, this exercise shows that the discussion presented in the main text is consistent with previous works.

-
- [1] R.D. Peccei and H.R. Quinn, *CP Conservation in the Presence of Instantons*, *Phys. Rev. Lett.* **38** (1977) 1440.
- [2] S. Weinberg, *A New Light Boson?*, *Phys. Rev. Lett.* **40** (1978) 223.
- [3] F. Wilczek, *Problem of Strong P and T Invariance in the Presence of Instantons*, *Phys. Rev. Lett.* **40** (1978) 279.
- [4] J. Preskill, M.B. Wise and F. Wilczek, *Cosmology of the Invisible Axion*, *Phys. Lett. B* **120** (1983) 127.
- [5] L.F. Abbott and P. Sikivie, *A Cosmological Bound on the Invisible Axion*, *Phys. Lett. B* **120** (1983) 133.
- [6] M. Dine and W. Fischler, *The Not So Harmless Axion*, *Phys. Lett. B* **120** (1983) 137.
- [7] P.W. Graham, D.E. Kaplan and S. Rajendran, *Cosmological Relaxation of the Electroweak Scale*, *Phys. Rev. Lett.* **115** (2015) 221801 [1504.07551].
- [8] A. Arvanitaki, S. Dimopoulos, V. Gorbenko, J. Huang and K. Van Tilburg, *A small weak scale from a small cosmological constant*, *JHEP* **05** (2017) 071 [1609.06320].
- [9] A. Banerjee, H. Kim and G. Perez, *Coherent relaxation dark matter*, *Phys. Rev. D* **100** (2019) 115026 [1810.01889].
- [10] A. Banerjee, H. Kim, O. Matsedonskyi, G. Perez and M.S. Safronova, *Probing the Relaxed Relaxion at the Luminosity and Precision Frontiers*, *JHEP* **07** (2020) 153 [2004.02899].
- [11] N. Arkani-Hamed, R.T. D’Agnolo and H.D. Kim, *Weak scale as a trigger*, *Phys. Rev. D* **104** (2021) 095014 [2012.04652].
- [12] R. Tito D’Agnolo and D. Teresi, *Sliding Naturalness: New Solution to the Strong-CP and Electroweak-Hierarchy Problems*, *Phys. Rev. Lett.* **128** (2022) 021803 [2106.04591].
- [13] R. Tito D’Agnolo and D. Teresi, *Sliding naturalness: cosmological selection of the weak scale*, *JHEP* **02** (2022) 023 [2109.13249].
- [14] A. Chatrchyan and G. Servant, *Relaxion Dark Matter from Stochastic Misalignment*, 2211.15694.
- [15] W. Hu, R. Barkana and A. Gruzinov, *Cold and fuzzy dark matter*, *Phys. Rev. Lett.* **85** (2000) 1158 [astro-ph/0003365].
- [16] L. Hui, *Wave Dark Matter*, *Ann. Rev. Astron. Astrophys.* **59** (2021) 247 [2101.11735].
- [17] H.-Y. Schive, T. Chiueh and T. Broadhurst, *Cosmic Structure as the Quantum Interference of a Coherent Dark Wave*, *Nature Phys.* **10** (2014) 496 [1406.6586].
- [18] H.-Y. Schive, M.-H. Liao, T.-P. Woo, S.-K. Wong, T. Chiueh, T. Broadhurst et al., *Understanding the Core-Halo Relation of Quantum Wave Dark Matter from 3D Simulations*, *Phys. Rev. Lett.* **113** (2014) 261302 [1407.7762].
- [19] L. Hui, J.P. Ostriker, S. Tremaine and E. Witten, *Ultralight scalars as cosmological dark matter*, *Phys. Rev. D* **95** (2017) 043541 [1610.08297].
- [20] N. Seto and A. Cooray, *Search for small-mass black hole dark matter with space-based gravitational wave detectors*, *Phys. Rev. D* **70** (2004) 063512 [astro-ph/0405216].
- [21] A.W. Adams and J.S. Bloom, *Direct detection of dark matter with space-based laser interferometers*, astro-ph/0405266.
- [22] E.D. Hall, R.X. Adhikari, V.V. Frolov, H. Müller, M. Pospelov and R.X. Adhikari, *Laser Interferometers as Dark Matter Detectors*, *Phys. Rev. D* **98** (2018) 083019 [1605.01103].
- [23] J. Jaeckel, S. Schenk and M. Spannowsky, *Probing dark matter clumps, strings and domain walls with gravitational wave detectors*, *Eur. Phys. J. C* **81** (2021) 828 [2004.13724].
- [24] S. Baum, M.A. Fedderke and P.W. Graham, *Searching for dark clumps with gravitational-wave detectors*, *Phys. Rev. D* **106** (2022) 063015 [2206.14832].
- [25] A. Sesana et al., *Unveiling the gravitational universe at μ -Hz frequencies*, *Exper. Astron.* **51** (2021) 1333 [1908.11391].
- [26] M.A. Fedderke, P.W. Graham and S. Rajendran, *Asteroids for μ Hz gravitational-wave detection*, *Phys. Rev. D* **105** (2022) 103018 [2112.11431].
- [27] M.A. Fedderke, P.W. Graham and S. Rajendran, *Gravity Gradient Noise from Asteroids*, *Phys. Rev. D* **103** (2021) 103017 [2011.13833].
- [28] J.I. Read, *The Local Dark Matter Density*, *J. Phys. G* **41** (2014) 063101 [1404.1938].
- [29] P.F. de Salas and A. Widmark, *Dark matter local density determination: recent observations and future prospects*, *Rept. Prog. Phys.* **84** (2021) 104901 [2012.11477].
- [30] R.-G. Cai, Z.-K. Guo, B. Hu, C. Liu, Y. Lu, W.-T. Ni et al., *On networks of space-based gravitational-wave detectors*, 2305.04551.
- [31] H. Kim and A. Lenoci, *Gravitational focusing of wave dark matter*, *Phys. Rev. D* **105** (2022) 063032 [2112.05718].
- [32] A. Derevianko, *Detecting dark-matter waves with a network of precision-measurement tools*, *Phys. Rev. A* **97** (2018) 042506 [1605.09717].

- [33] J.W. Foster, N.L. Rodd and B.R. Safdi, *Revealing the Dark Matter Halo with Axion Direct Detection*, *Phys. Rev. D* **97** (2018) 123006 [1711.10489].
- [34] G.P. Centers et al., *Stochastic fluctuations of bosonic dark matter*, *Nature Commun.* **12** (2021) 7321 [1905.13650].
- [35] M. Otto, *Time-Delay Interferometry Simulations for the Laser Interferometer Space Antenna*, Ph.D. thesis, Leibniz U., Hannover, 2015. 10.15488/8545.
- [36] M. Tinto and S.V. Dhurandhar, *Time-delay interferometry*, *Living Rev. Rel.* **24** (2021) 1.
- [37] M. Tinto and J.W. Armstrong, *Cancellation of laser noise in an unequal-arm interferometer detector of gravitational radiation*, *Phys. Rev. D* **59** (1999) 102003.
- [38] J.W. Armstrong, F.B. Estabrook and M. Tinto, *Time-Delay Interferometry for Space-based Gravitational Wave Searches*, *Astrophys. J.* **527** (1999) 814.
- [39] S. Babak, A. Petiteau and M. Hewitson, *LISA Sensitivity and SNR Calculations*, 2108.01167.
- [40] M. Maggiore, *Gravitational Waves. Vol. 1: Theory and Experiments*, Oxford Master Series in Physics, Oxford University Press (2007).
- [41] S. Phinney et al, *The Big Bang Observer: Direct Detection of Gravitational Waves from the Nirth of the Universe to the Presen*, *NASA Mission Concept Study* (2004) .
- [42] ALIGO collaboration, *Sensitivity and performance of the Advanced LIGO detectors in the third observing run*, *Phys. Rev. D* **102** (2020) 062003 [2008.01301].
- [43] S. Hild et al., *Sensitivity Studies for Third-Generation Gravitational Wave Observatories*, *Class. Quant. Grav.* **28** (2011) 094013 [1012.0908].
- [44] LISA collaboration, *Laser Interferometer Space Antenna*, 1702.00786.
- [45] M. Armano et al., *Sub-Femto- g Free Fall for Space-Based Gravitational Wave Observatories: LISA Pathfinder Results*, *Phys. Rev. Lett.* **116** (2016) 231101.
- [46] M. Armano et al., *Beyond the Required LISA Free-Fall Performance: New LISA Pathfinder Results down to 20 μ Hz*, *Phys. Rev. Lett.* **120** (2018) 061101.
- [47] T. Robson, N.J. Cornish and C. Liu, *The construction and use of LISA sensitivity curves*, *Class. Quant. Grav.* **36** (2019) 105011 [1803.01944].
- [48] N.J. Cornish, *Detecting a stochastic gravitational wave background with the Laser Interferometer Space Antenna*, *Phys. Rev. D* **65** (2002) 022004 [gr-qc/0106058].
- [49] N. Cornish and T. Robson, *Galactic binary science with the new LISA design*, *J. Phys. Conf. Ser.* **840** (2017) 012024 [1703.09858].
- [50] J. Crowder and N.J. Cornish, *Beyond LISA: Exploring future gravitational wave missions*, *Phys. Rev. D* **72** (2005) 083005 [gr-qc/0506015].
- [51] K. Yagi and N. Seto, *Detector configuration of DECIGO/BBO and identification of cosmological neutron-star binaries*, *Phys. Rev. D* **83** (2011) 044011 [1101.3940].
- [52] B. Bar-Or, J.-B. Fouvy and S. Tremaine, *Relaxation in a Fuzzy Dark Matter Halo*, *Astrophys. J.* **871** (2019) 28 [1809.07673].
- [53] N.P. Pitjev and E.V. Pitjeva, *Constraints on dark matter in the solar system*, *Astron. Lett.* **39** (2013) 141 [1306.5534].
- [54] S.L. Adler, *Placing direct limits on the mass of earth-bound dark matter*, *J. Phys. A* **41** (2008) 412002 [0808.0899].
- [55] LIGO SCIENTIFIC, VIRGO collaboration, *Improved Upper Limits on the Stochastic Gravitational-Wave Background from 2009–2010 LIGO and Virgo Data*, *Phys. Rev. Lett.* **113** (2014) 231101 [1406.4556].
- [56] LIGO SCIENTIFIC, VIRGO collaboration, *Searching for stochastic gravitational waves using data from the two colocated LIGO Hanford detectors*, *Phys. Rev. D* **91** (2015) 022003 [1410.6211].
- [57] M. Tinto, J.W. Armstrong and F.B. Estabrook, *Discriminating a gravitational wave background from instrumental noise in the LISA detector*, *Phys. Rev. D* **63** (2001) 021101.
- [58] C.J. Hogan and P.L. Bender, *Estimating stochastic gravitational wave backgrounds with Sagnac calibration*, *Phys. Rev. D* **64** (2001) 062002 [astro-ph/0104266].
- [59] J.D. Romano and N.J. Cornish, *Detection methods for stochastic gravitational-wave backgrounds: a unified treatment*, *Living Rev. Rel.* **20** (2017) 2 [1608.06889].
- [60] A. Banerjee, D. Budker, J. Eby, H. Kim and G. Perez, *Relaxion Stars and their detection via Atomic Physics*, *Commun. Phys.* **3** (2020) 1 [1902.08212].
- [61] A. Banerjee, D. Budker, J. Eby, V.V. Flambaum, H. Kim, O. Matsedonskyi et al., *Searching for Earth/Solar Axion Halos*, *JHEP* **09** (2020) 004 [1912.04295].
- [62] D. Budker, J. Eby, M. Gorghetto, M. Jiang and G. Perez, *A Generic Formation Mechanism of Ultralight Dark Matter Solar Halos*, 2306.12477.
- [63] A. Khmelnitsky and V. Rubakov, *Pulsar timing signal from ultralight scalar dark matter*, *JCAP* **02** (2014) 019 [1309.5888].
- [64] H. Kim and A. Mitridate, *to appear*, .
- [65] M. Maggiore, *Gravitational Waves. Vol. 2: Astrophysics and Cosmology*, Oxford University Press (3, 2018).